

Analysis and Forecasting of the Dynamics of a Floating Wind Turbine Using Dynamic Mode Decomposition

Giorgio Palma*, Andrea Bardazzi, Alessia Lucarelli, Chiara Pilloton, Andrea Serani,
Claudio Lugni, Matteo Diez

National Research Council-Institute of Marine Engineering, Rome, Italy

*giorgio.palma@cnr.it

ABSTRACT

This article presents a data-driven equation-free modeling of the dynamics of a hexafloat floating offshore wind turbine based on the Dynamic Mode Decomposition (DMD). The DMD is here used to provide a modal analysis and extract knowledge from the dynamic system. A forecasting algorithm for the motions, accelerations, and forces acting on the floating system, as well as the height of the incoming waves, the wind speed, and the power extracted by the wind turbine, is developed by using a methodological extension called Hankel-DMD, that includes time-delayed copies of the states in an augmented state vector. All the analyses are performed on experimental data collected from an operating prototype. The quality of the forecasts obtained varying two main hyperparameters of the algorithm, namely the number of delayed copies and the length of the observation time, is assessed using three different error metrics, each analyzing complementary aspects of the prediction. A statistical analysis exposed the existence of optimal values for the algorithm hyperparameters. Results show the approach's capability for short-term future estimates of the system's state, which can be used for real-time prediction and control. Furthermore, a novel Stochastic Hankel-DMD formulation is introduced by considering hyperparameters as stochastic variables. The stochastic version of the method not only enriches the prediction with its related uncertainty but is also found to improve the normalized root mean square error up to 10% on a statistical basis compared to the deterministic counterpart.

Keywords Dynamic Mode Decomposition · Data-driven modeling · Digital twinning · Forecasting · Floating Offshore Wind Turbine

1 Introduction

In the strive of containing the global temperature increase under 2°C below pre-industrial levels, as set by the Paris Agreement [19], most countries have committed to reaching the goal of *net zero emissions* by 2050, meaning that all the greenhouse gas emissions must be counterbalanced by an equal amount of removals from the atmosphere. To reach this critical and ambitious task for sustainable growth, the decarbonization of our society is a key aspect that passes through the decarbonization of energy production [44, 26]. The shift from fossil fuels to renewable sources for power production is to be considered the fundamental step in the process. Power generation is, in fact, responsible for 30% of the global carbon dioxide emissions at the moment. In 2018, the European Union set intermediate targets of 20% of energy obtained from renewable resources by 2020 and 32% by 2030, the latter has been raised to 42.5% (with the aspiration of reaching 45%) by amending the Renewable Energy Directive in 2021 [68]. Reaching the mentioned targets means almost doubling the existing share of renewable energy in the EU.

Wind energy technology has been identified as one of the most promising ones, along with photovoltaic, for power production from renewable sources. Several growth scenarios predict a prominent role of wind power,

exceeding the 35% share of the total electricity demand by 2050 [47], representing a nearly nine-fold rise in the wind power share in the total generation mix compared to 2016 levels. Offshore wind energy production has a bigger growth potential compared to its onshore counterpart. The reasons are connected to fewer technical, logistic, and social restrictions of the former. Offshore installed turbines may exploit abundant and more consistent winds, helped by the reduced friction of the sea surface and the absence of surrounding hills and buildings [31]. In addition, offshore wind farms benefit a greater social acceptance, a minor value of their occupied space, and the possibility of installing larger turbines with fewer transportation issues than onshore [49, 50, 39]. The 2023 Global Offshore Wind Report predicts the installation of more than 380 GW of offshore wind capacity worldwide in the next ten years [9]. The exponential growth of the sector passes through the possibility of realizing floating offshore plants, enabling the exploitation of sea areas with deeper water that make fixed-foundation turbines not a feasible/affordable solution (indicatively deeper than 60 m). The main advantage of exploiting deep offshore sea areas relies on the abundant and steady winds characterizing them. One of the main limiting factors in the reduction of the levelized cost of energy (LCOE) of advanced floating offshore wind turbines (FOWTs) is the current size and cost of their platforms. Its reduction, alongside the development of advanced moorings, improved control systems, and maintenance procedures is among the most impacting technical goals research activities are focusing on. The power production by FOWTs presents additional challenges compared to the fixed wind turbine counterpart (on- or offshore) which are inherent to their floating characteristic that adds six degrees of freedom to the structures. Nonlinear hydrodynamic loads, wave-current interactions, aero-hydrodynamics coupling producing negative aerodynamic damping, and wind-induced low-frequency rotations are among the main causes of large amplitude motions of the platform. These are in turn causes of a reduction in the average power output of the power plant and of an increase in the fluctuations of the produced power. Both quantity and quality of the power production are affected and the structure and all the components (blades, cables, bearings, etc.) also suffer increased fatigue-induced wear from non-constant loadings [43] (about 20% of operation and maintenance costs come from blade failures [20] and almost 70% of the gearbox downtime is due to bearing faults [10]).

The floating wind turbine operations are considerably altered by the stochastic nature of wind, waves, and currents in the sea environment, which excite platform motion leading to uncertainties in structural loads and power extraction capability. As shown first in [27], waves are responsible for a large part of the dynamic excitation of a FOWT. Rotor speed fluctuations are 60% larger when the same turbine is operated in a floating environment compared to onshore installation, and the difference has been shown to increase with increasing wave conditions. Therefore, it is essential to develop appropriate strategies to improve the FOWTs' platform stability and maximize the turbines' energy conversion rate, achieving better LCOE with higher power production and lower maintenance operation costs. Both passive and active technologies have been studied and developed to the scope, such as tuned mass dampers [63, 37, 14] mounted on different floaters, ballasted buoyancy cans [67, 22, 23], gyro-stabilizers [45], blade pitch and/or torque controllers [39, 56, 69, 49, 50]. Developing advanced control systems is a high-potential cost reduction strategy for offshore wind turbines impacting at multiple levels: effective control strategies may increase the energy production which has a direct impact on LCOE; a reduction of the platform motions may help in reducing their sizes and costs; reduced vibratory loads on the turbine's components helps increasing their lifetime and reducing maintenance costs. A thorough comparison of various controllers designed for managing vibratory loads is provided in [2]. Among all the methods analyzed, the strategies that employ blade pitch control, collective or individual, emerge as the most effective and promising, combining feasibility and reliability. Particular care must be taken in floating systems when applying controls: closed-loop instability may be induced by the coupling between the motions of the platform (particularly pitch dynamics) and the aerodynamic loads [35, 28] for poorly designed controllers acting on the pitch of the blades.

In floating wind turbines, power production, load reduction, pitch activity, and platform stabilization are multiple conflicting objectives the controller has to deal with, and a trade-off between the opposing needs is to be found [36]. Traditional control algorithms (PI, Gain Scheduled PI, PID) are typically of single-input-single-output type and struggle to deal with multiple objectives [35, 28, 72, 36]. Optimal algorithms, such as linear quadratic regulator [49, 57], model predictive control [71], and H_2 and H_∞ methods [3, 5] have also been applied to FOWT with good results overcoming the mentioned issue, but at the cost of an increased controller design complexity. Recently, a multi-objective multilayer control algorithm was proposed in [50], combining two resonant controllers based on collective pitch actuation and a proportional-integral controller providing the blade cyclic pitch. The authors demonstrated the strategy to effectively reject the vibratory loads induced by the sea waves, and reduce the blade root loads at the rotor revolution frequency and the floater motions. However, high pitch rates and actuation power were found to be needed for individual pitch control.

All the mentioned strategies work with a feedback loop on the actuation variable. On the other side, there is the feedforward control system, often coupled with model predictive control, which is based on knowledge about the dynamic system in the form of a predictive model and the disturbances it experiences. The two philosophies may also be effectively coupled, creating a feedforward control with a feedback loop such as in [1], where real-time prediction of the free-surface elevation is exploited to compensate for the wave disturbances on the FOWT. The wave-induced rotor speed variations, and consequently structural loads on the turbine, are successfully reduced in a high-fidelity simulated environment. Feedforward controllers have been deemed and demonstrated to be effective strategies for further improving the control of FOWTs [24, 34, 15, 16, 17, 64]. A collective pitch feedforward controller was designed in [58] showing the ability to regulate rotor speed under an extreme gust, using information about the wind field by a LIDAR (light detection and ranging) system virtually mounted on the turbine's nacelle. The methodology was extended to a model predictive individual pitch control in [51]. In general, the availability of environmental data to the controller enhances its control action capability: the use of information about incoming waves to design a feedforward control strategy for a 10MW FOWT is presented in [21], showing improved quality of the produced power, and increased turbine fatigue life. In [40], a finite-horizon LQR (linear-quadratic regulator) controller is designed using wave elevation and forces data from a real-time forecasting algorithm. The controller is applied to a tension-leg platform FOWT to mitigate structural loads on the tower.

Such feedforward algorithms rely on forecasting techniques to estimate upcoming disturbances or changes in the state to be controlled. Hence, the predictive algorithm is invested of a primary role in the success of the control strategy. Several machine learning algorithms have been implemented in the literature to predict relevant quantities for FOWT and control. In [53], the delay introduced by the hydraulic actuator of the blades' pitch angle control is addressed. The blade pitch angle is predicted by a long short-term memory neural network and its signal is exploited to compensate for the actuation delay, resulting in improved control performances. In [40], two different forecasting algorithms are developed to predict the wave elevation and feed a feedforward LQR controller: one is based on the Prony method and identifies the signal as a sum of exponentials; the other uses Least-squares Support Vector Machines regression to estimate the forecasted signal from a high dimensional feature space of the input vector. The study in [4] adopts a convolutional neural network merged with a gated recurrent unit network for the forecasting of the dynamic behavior of FOWTs. Albeit powerful, machine learning and deep learning methods typically require large training datasets, comprising a range of operating conditions as complete as possible to learn patterns that generalize to *new* situations. The training of such algorithms can be computationally expensive, and typically not compatible with real-time learning and digital twinning, where the system characteristics and response to external perturbations change with the system aging.

The objective of this paper is to explore the usage of Dynamic Mode Decomposition (DMD) as a method to extract knowledge and develop a forecasting algorithm for relevant quantities of a FOWT from experimental data, avoiding the shortcomings of machine learning approaches to obtain a continuously learning reduced order model more suitable for digital twinning. DMD is a powerful data-driven technique used for analyzing the temporal evolution of complex systems. It was originally developed in the field of fluid dynamics where it has been employed to identify coherent structures, *e.g.* in vorticity generated by bluff bodies [66], jet turbulence [60], noise generated in jets mixing layers [65], and predict their evolution or perform stability analysis of complex flows [54, 59] and magnetized plasma [30]. DMD has then found applications in various scientific and engineering domains, including structural dynamics, epidemiology analyses [48], and neuroscience [6] extracting spatial-temporal coherent patterns in large-scale neural recordings. At its core, DMD extracts coherent spatiotemporal patterns from high-dimensional data, and it has been originally introduced as a method to identify linear normal modes in linear systems. The DMD has then evolved to capture the underlying dynamics and coherent structures of complex, nonlinear systems, leveraging the concept of the Koopman operator. As a main characteristic, the DMD is an equation-free and data-driven method, operating on measured or simulated data without requiring detailed knowledge of the equations governing the evolution of the state of the system under analysis. DMD doesn't assume any specific system dynamics; instead, it uncovers underlying structures directly from the data. This makes DMD particularly well-suited for practical applications, where obtaining a precise mathematical model is challenging or impractical, contributing to its growing success in the scientific community in several fields [8]. Given a time series of data, the DMD computes a set of modes and frequencies approximating the eigenmodes and eigenvalues of the Koopman operator (also called the composition operator), an infinite-dimensional linear operator associated with the time evolution of the system under analysis, even in the presence of nonlinearities. Some main challenges have to be addressed in using the algorithm: i) DMD is sensitive to noise in the data, which deteriorates its capability of mode extraction and hence predictive ability; ii) DMD relies on Krylov subspaces for model approximation, which proper closure is challenging in nonlinear

systems: if the system exhibits strong nonlinear behavior, DMD may struggle to capture all relevant modes. Despite these limitations, DMD remains a valuable tool for extracting patterns from time series data.

The modes and frequencies identified by the DMD may also be used to build a predictive model of the system under analysis. Compared to the other applications, the literature about time series forecasting by using DMD is less extensive. Nevertheless, interesting applications in very different fields can be found: an algorithmic trading strategy based on DMD is demonstrated in [41], allowing for a prediction of the market dynamics to inform a financial investment strategy; the work in [18] describes a power systems engineering application in which a model able to forecast power grid loads is obtained by applying the DMD with state augmentations; the analysis and forecast of the trajectories/motions/forces of ships operating in waves is presented in [12, 62], where the DMD is employed to produce short-term future estimates of the system's state, suggesting the relevance for real-time prediction and control; the same naval application is studied in [13] developing a hybrid prediction algorithm combining DMD and artificial neural network, and in [11] comparing the performances of different neural network architecture and a DMD implementation using an augmented state by embedding delayed time histories and time derivatives. All the mentioned works show promising results and good prediction capabilities in short-term and medium-term perspectives with accuracy and reduced computational effort.

The DMD does not fall under the category of machine learning techniques, however, the machine learning terminology can be borrowed to highlight some peculiarity of the method. In this view, the evaluation of the DMD modes and frequencies can be called the *training phase*, and the time signals to feed the algorithm the *training set*. The main advantage of the DMD over proper machine learning and deep learning methods is its one-shot training time and corresponding lower computational cost, only related to direct linear algebra operations as detailed in Section 2.2. The DMD is inherently suitable for continuous learning, and its system identification naturally adapts to a changing system and environment, making it a promising tool also in the context of digital twins.

In this paper, for the first time to the best of the authors' knowledge, the DMD is used to improve knowledge and develop a forecasting algorithm for relevant quantities of a FOWT. In particular, a methodology extension of the DMD, called Hankel-DMD (HDMD) (also called Augmented DMD or delay DMD) [7, 29, 62] is applied to this scope. This specific version of the DMD algorithm has been developed to deal with the cases in which only partial observations of the system are available such that there are *latent* variables. The state vector is thus augmented, embedding time-delayed copies of the original variables, resulting in an intrinsic coordinate system that forms a Koopman-invariant subspace (the time-delays form a set of observable functions that span a finite-dimensional subspace of Hilbert space, in which the Koopman operator preserves the structure of the system) [7, 46]. The method is applied to real-life measured data obtained by various sensors mounted on the floating platform and the turbine, focusing on short-term and medium-term prediction horizons using the incoming wave period as a reference. The experimental activity has been conducted on a scale prototype of a 5MW Hexafloat FOWT, the first of its type, as part of the National Research Project *RdS-Electrical Energy from the Sea*, funded by the Italian Ministry for the Environment (MaSE) and coordinated by CNR-INM. Two main hyperparameters of the algorithm and their effect on the predictions in the studied case are studied and discussed by testing a full-factorial combination of the setting parameters. To this aim, three evaluation metrics are statistically assessed for each combination against a relevant number of time sequences samples, randomly extracted from the data record. Moreover, a stochastic version of the Hankel-DMD (SHDMD) is obtained by considering the hyperparameters as random variables with uniform distribution in a suitable range, obtaining a mean prediction with associated uncertainty. It is finally shown that the application of the SHDMD leads to improved predictive performances compared to the deterministic counterpart.

The paper is organized as follows. Section 2 presents the wind turbine test case, details the DMD methods applied, and introduces the performance metrics used to assess the predictive performances of the algorithms. The numerical setup and the data preprocessing are described in Section 3. Section 4 collects the results from the modal analysis and the forecasting of the quantities of interest obtained with the deterministic Hankel-DMD and its stochastic version. Finally, conclusions about the conducted analyses are resumed in Section 5.

2 Material and methods

2.1 Wind turbine test case

The presented analyses are conducted on a set of experimental data collected on the prototype of a FOWT built and tested at the Interdisciplinary Marine Renewable Energy sea Lab (In-MaRELab), see Figure 1a, offshore the Naples port, right in front of the breakwater Molo San Vincenzo. The prototype and the

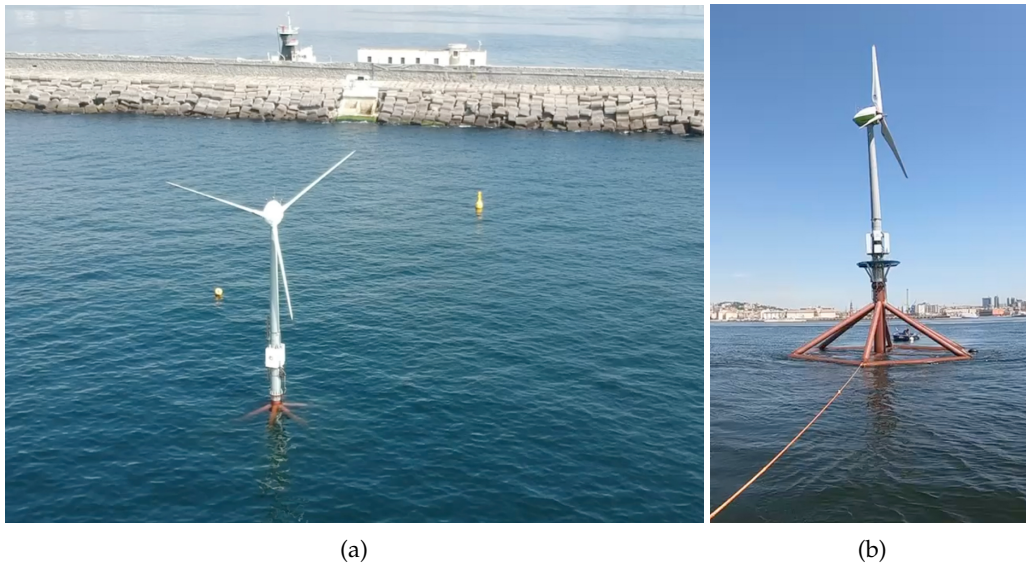


Figure 1: (a) Aerial view of In-MaRELab with the Hexafloat FOWT during the tests at sea in 2021. (b) View of the Hexafloat FOWT during the towing stage from the shipyard to the test site in 2024.

experimental activity at sea are part of the National Research Project *RdS-Electrical Energy from the Sea*, funded by the Italian Ministry for the Environment (MaSE) and coordinated by CNR-INM. The FOWT is a 1:6.8 scale prototype of a 5MW FOWT, the first one existing at sea for the Hexafloat concept. The floater is a Saipem patented lightweight semisub platform consisting of a hexagonal tubular steel structure around a central column, and a deeper counterweight, connected to the floater by six tendons (one for each corner of the hexagon) in synthetic material. The floater hosts a Tozzi Nord TN535 10-kW wind turbine [52], originally designed for onshore application and, within the present RP, suitably modified on the electrical part for the specific aims of the offshore application (see Figure 1b).

The FOWT is anchored with three drag anchors located at 30 m of water depth through three mooring lines in catenary configuration at a relative angle of 120 degrees counterclockwise, with M_1 directed towards the breakwater and orthogonal to it.

The studied dataset includes 12-hour synchronized time histories of

1. the loads applied to one of the three moorings of the platform (M_3), and three of the six tendons connecting the counterweight to the floater (T_1 , T_5 , and T_6), as measured by a system of underwater load cells LCM5404 with work limit load (WLL) of 2.3 tons and 4.5 tons, respectively;
2. the acceleration along three coordinate axes (\dot{u} , \dot{v} , \dot{w}), the pitch and roll angles (θ , ϕ), and the respective angular rates ($\dot{\theta}$, $\dot{\phi}$), collected by the Norwegian Subsea MRU 3000 inertial motion unit;
3. the power extracted by the wind turbine (P), estimated by a PLC through a direct measure of the electrical quantities at the generator on board the nacelle of the wind turbine, the rotor angular velocity (Ω) measured by two sensors in continuous cross-check, the relative wind speed (V_w) through two different anemometers positioned on the nacelle, behind the rotor. All signals were collected by the PLC on the nacelle with a variable but well-known sample frequency of approximately 1 Hz;
4. the wave elevation (h_w) measured by a pressure transducer integrated into the Acoustic Doppler Current Profiler Teledyne Marine-Sentinel V20, located at a distance of approximately 50 m from the FOWT in the SE direction.

The state of the system is hence composed as $\mathbf{x} = \{T_1, T_5, T_6, M_3, \phi, \theta, \dot{\phi}, \dot{\theta}, \dot{u}, \dot{v}, \dot{w}, P, \Omega, V_w, h_w\}$.

The data consider a window of continuous operations in extreme weather conditions. The system may show induced strongly non-linear physical dynamics in such weather conditions. In particular, the intense wind causes a nonlinear behavior in the extracted power and blades' rotating speed, showing a saturation to the maximum values supported by the machine. This poses the DMD-based methods in a challenging condition for modal analysis and prediction.

An average incoming wave period is identified from the peak in the wave elevation spectrum and used in the following as reference period $\hat{T} = 7.3143 \text{ s}$ ($\hat{f} = 0.1367 \text{ Hz}$).

2.2 Dynamic Mode Decomposition

The DMD was originally developed to identify spatiotemporal coherent structures from high-dimensional time series data, providing a linear reduced-order representation of a possibly nonlinear system dynamics through a set of modes with associated oscillation frequencies and decay/growth rates [8]. When the analyzed system is linear, the modes obtained by the DMD correspond to the system's linear normal modes. The potential of the DMD in the analysis of nonlinear systems comes from its close relation to the spectral analysis of the Koopman operator[55], which is a linear operator that captures the evolution of observables describing a possibly nonlinear dynamical system[70]. The DMD analysis approximates the eigenmodes and eigenvalues of the infinite-dimensional linear Koopman operator, associated with the evolution over time of the system at hand, thus providing a linearized finite-dimensional representation of the dynamics of the nonlinear original system [33].

Consider a dynamical system described by

$$\frac{d\mathbf{x}}{dt} = \mathbf{f}(\mathbf{x}, t, \gamma) \quad (1)$$

where $\mathbf{x}(t) \in \mathcal{R}^n$ represents the system's state at time t , γ contains the parameters of the system, and $\mathbf{f}(\cdot)$ represents its dynamics. In typical applications, the state \mathbf{x} may represent the discretization of a partial differential equation at several spatial points, or be composed by multiple-variable time series of a dynamical system, and thus is generally large with $n \gg 1$. Approximating Eq. (1) with DMD leads to a locally linear dynamical system defined as

$$\frac{d\mathbf{x}}{dt} = \mathcal{A}\mathbf{x} \quad (2)$$

which solution can be expressed in terms of eigenvalues ω_k and eigenvectors ϕ_k of the matrix \mathcal{A}

$$\mathbf{x}(t) = \sum_{k=1}^n \phi_k q_k(t) = \sum_{k=1}^n \phi_k b_k \exp(\omega_k t), \quad (3)$$

where the coefficients b_k are the coordinates of the initial condition \mathbf{x}_0 in the eigenvector basis, $\mathbf{b} = \Phi^{-1}\mathbf{x}_0$

In practical applications, the state of the system is measured at m discrete time steps with sampling time Δt and can be expressed as $\mathbf{x}_j = \mathbf{x}(j\Delta t)$ with $j = 1, \dots, m$. This data is governed by a discrete-time dynamical system, equivalent to the one of Eq. (1)

$$\mathbf{x}_{j+1} = \mathbf{F}(\mathbf{x}_j, j, \gamma) \quad (4)$$

Equivalently, the DMD approximation can be written as

$$\mathbf{x}_{j+1} = \mathbf{A}\mathbf{x}_j, \quad \text{with} \quad \mathbf{A} = \exp(\mathcal{A}\Delta t) \quad (5)$$

For each time step j , a snapshot of the system is defined as the column vector collecting the measured full state of the system \mathbf{x}_j . Two matrices can be obtained by arranging the available snapshots as follows

$$\mathbf{X} = [\mathbf{x}_1 \quad \mathbf{x}_2 \quad \dots \quad \mathbf{x}_{m-1}], \quad \mathbf{X}' = [\mathbf{x}_2 \quad \mathbf{x}_3 \quad \dots \quad \mathbf{x}_m] \quad (6)$$

such that Eq. (5) may be written in terms of these data matrices

$$\mathbf{X}' \approx \mathbf{A}\mathbf{X} \quad (7)$$

Hence, the matrix \mathbf{A} can be constructed using the following approximation

$$\mathbf{A} \approx \mathbf{X}'\mathbf{X}^\dagger \quad (8)$$

where \mathbf{X}^\dagger is the Moore-Penrose pseudoinverse of \mathbf{X} , which minimize $\|\mathbf{X}' - \mathbf{A}\mathbf{X}\|_F$, where $\|\cdot\|_F$ is the Frobenius norm. The pseudoinverse of \mathbf{X} can be efficiently evaluated using the singular value decomposition (SVD) as $\mathbf{X}^\dagger = \mathbf{V}\mathbf{\Sigma}^{-1}\mathbf{U}^*$, where $*$ denotes the complex conjugate transpose. The matrix $\tilde{\mathbf{A}}$ is evaluated projecting \mathbf{A} onto the POD modes in \mathbf{U}

$$\tilde{\mathbf{A}} = \mathbf{U}^* \mathbf{A} \mathbf{U}, \quad (9)$$

and its spectral decomposition can be evaluated

$$\tilde{\mathbf{A}} \mathbf{W} = \mathbf{W} \mathbf{\Lambda} \quad (10)$$

The diagonal matrix $\mathbf{\Lambda}$ contains the DMD eigenvalues λ_k , while the DMD modes ϕ_k constituting the matrix $\mathbf{\Phi}$ are then reconstructed using the eigenvectors \mathbf{W} and the time-shifted data matrix \mathbf{X}' (this algorithm is referred to as the exact-DMD [70])

$$\mathbf{\Phi} = \mathbf{X}' \mathbf{V} \mathbf{\Sigma}^{-1} \mathbf{W} \quad (11)$$

The state-variable evolution in time can be approximated by the modal expansion of Eq. (3), where $\omega_k = \ln(\lambda_k)/\Delta t$, starting from an initial condition corresponding to the end of the measured data $\mathbf{b} = \mathbf{\Phi}^{-1} \mathbf{x}_m$.

2.3 Hankel-DMD

In this work, an extension of the DMD algorithm is applied for the forecasting of the variables from the wind turbine dataset, called Hankel-DMD [7, 29]. The Hankel-DMD involves extending the original state by embedding a set of d time-delayed copies of it in the state vector. A single time step separates two subsequent shifted copies, and the resulting modified data matrices are organized in the form of two Hankel matrices

$$\hat{\mathbf{X}} = \begin{bmatrix} \mathbf{x}_{d+1} & \mathbf{x}_{d+2} & \cdots & \mathbf{x}_{m-1} \\ \mathbf{x}_d & \mathbf{x}_{d+1} & \cdots & \mathbf{x}_{m-2} \\ \vdots & \vdots & \vdots & \vdots \\ \mathbf{x}_1 & \mathbf{x}_2 & \cdots & \mathbf{x}_{m-1-d} \end{bmatrix}, \quad \hat{\mathbf{X}}' = \begin{bmatrix} \mathbf{x}_{d+2} & \mathbf{x}_{d+3} & \cdots & \mathbf{x}_m \\ \mathbf{x}_{d+1} & \mathbf{x}_{d+2} & \cdots & \mathbf{x}_{m-1} \\ \vdots & \vdots & \vdots & \vdots \\ \mathbf{x}_2 & \mathbf{x}_3 & \cdots & \mathbf{x}_{m-d} \end{bmatrix} \quad (12)$$

The only modification in the algorithm for the eigenvalue and eigenvector identification is, hence, the use of the augmented data matrices instead of the original in Eq. (6) and following.

The use of time-delayed copies as additional observables in the DMD has been connected to the Koopman operator as a universal linearizing basis [7]. When the rank of the data matrix (typically the length of its column vectors) is small, time-delayed copies are useful for augmenting it and thus the number of SVD modes that can be used for the dynamics modeling by the DMD, which can improve the accuracy of the prediction.

2.4 Stochastic Hankel-DMD

A Stochastic extension of the Hankel-DMD (SHDMD) is introduced, by assignigng the relevant DMD hyperparameters' suitably defined probability density functions. Here, both the observation time, $m\Delta t$, and the delay, $d\Delta t$ used to build the Hankel matrices in Eq. 12 are used as stochastic variables in the forecasting process. Sampling of the probability densities by the Monte Carlo method is performed, providing in output the mean prediction and its standard deviation, see [61].

2.5 Performance metrics

Three error indices are used to compare the effectiveness of the proposed DMD approach and setups to forecast the wind turbine data: the normalized mean square error (NRMSE), the normalized average minimum/maximum absolute error (NAMMAE), and the Jensen-Shannon Divergence (JSD). All the metrics are averaged over the variables constituting the system's state, to provide an overall assessment of the prediction accuracy and constitute a comprehensive evaluation by considering different aspects such as overall error, range of predicted and measured values, and correlation.

The NRMSE measures the average root mean square error between the predicted values \tilde{x}_t and the measured (test) values x_t at the various time steps. It is computed through the square root of the average squared differences, normalized by the standard deviation of the measured values:

$$\text{NRMSE} = \frac{1}{N} \sum_{i=1}^N \sqrt{\frac{1}{\mathcal{T} \sigma_{x_i}^2} \sum_{j=1}^{\mathcal{T}} (\tilde{x}_{ij} - x_{ij})^2} \quad (13)$$

where N is the number of variables in the predicted state, \mathcal{T} is the number of considered time instants, and σ_{x_i} is the standard deviation of the measured values in the considered time window for the variable x_i .

The NAMMAE metric, introduced in [13, 11], provides an engineering-oriented assessment of the prediction accuracy. It measures the absolute difference between the minimum and maximum values of the predicted and measured time series, as follows:

$$\text{NAMMAE} = \frac{1}{2N\sigma_{x_i}} \sum_{i=1}^N \left(\left| \min_j(\tilde{x}_{ij}) - \min_j(x_{ij}) \right| + \left| \max_j(\tilde{x}_{ij}) - \max_j(x_{ij}) \right| \right) \quad (14)$$

Lastly, the JSD measures the similarity between the probability distribution of the predicted and observed signal [42]. For each variable, it estimates the entropy of the predicted time series probability density function Q relative to the probability density function of the measured time series R , where M is the average of the two [38]. The Jensen-Shannon divergence is based on the Kullback-Leibler divergence D , given by Eq. (16), which is the expectation of the logarithmic difference between the probabilities K and H , both defined over the domain χ , where the expectation is taken using the probabilities K . [32].

$$\text{JSD} = \frac{1}{N} \sum_{i=1}^N \left(\frac{1}{2} D(Q_i || M_i) + \frac{1}{2} D(R_i || M_i) \right), \quad \text{with} \quad M = \frac{1}{2}(Q + R) \quad (15)$$

$$D(K || H) = \sum_{y \in \chi} K(y) \ln \left(\frac{K(y)}{H(y)} \right) \quad (16)$$

The similarity between the distributions is greater when the Jensen-Shannon distance is closer to zero and it is upper bounded by $\ln(2)$

The NRMSE has a subtle behavior that may mislead the interpretation of the results if used alone: with standardized data, a prediction that immediately goes to zero will produce an NRMSE close to the standard deviation of the observed signal (*i.e.*, around 1). This may be lower, for example, than the error obtained with a prediction well capturing the trend of the observed time history but with a small phase shift, and be misleading on the real forecasting capability of the algorithm at hand. The introduction of NAMMAE and JSD helps to discriminate the mentioned situation since their values would be higher for the null prediction instead.

3 Numerical setup

This section presents the the DMD setup, along with the preprocessing applied to the data, and the workflow for the DMD analysis and prediction. Figure 2 shows a sketch of the DMD modeling approach. The DMD is not a machine learning method in the strictest sense, however, a machine learning terminology and approach can be used when dealing with DMD due to its data-driven nature for time series prediction. The observed data can hence be called *training* or *test* depending on their time positioning to the DMD prediction starting point. Here the matrix \mathbf{A} is constructed using observed (past) time histories, which are used as a training set. When used for forecasting, the DMD-predicted time histories of the states are then compared against true observed (future) data used as a test set. All DMD analyses are based on normalized data. Specifically, the Z-score is used, therefore time histories with zero mean and unit variance are evaluated through the process.

Figure 3 offers a view of the workflow of the DMD analysis. The very first operation is the extraction of the time series from the dataset, using a sampling rate $dt = 0.1$ s. Then, data are fed to the preprocessing step, which output is constituted by the matrices $\hat{\mathbf{X}}$ and $\hat{\mathbf{X}}'$. It is well known that the accuracy of the DMD and derived algorithms rapidly deteriorates in the presence of noise in the data. For this reason, after the z-scoring, a low-pass filter with cutoff frequency $f_c = 0.5$ Hz is applied independently to the time series of each variable.

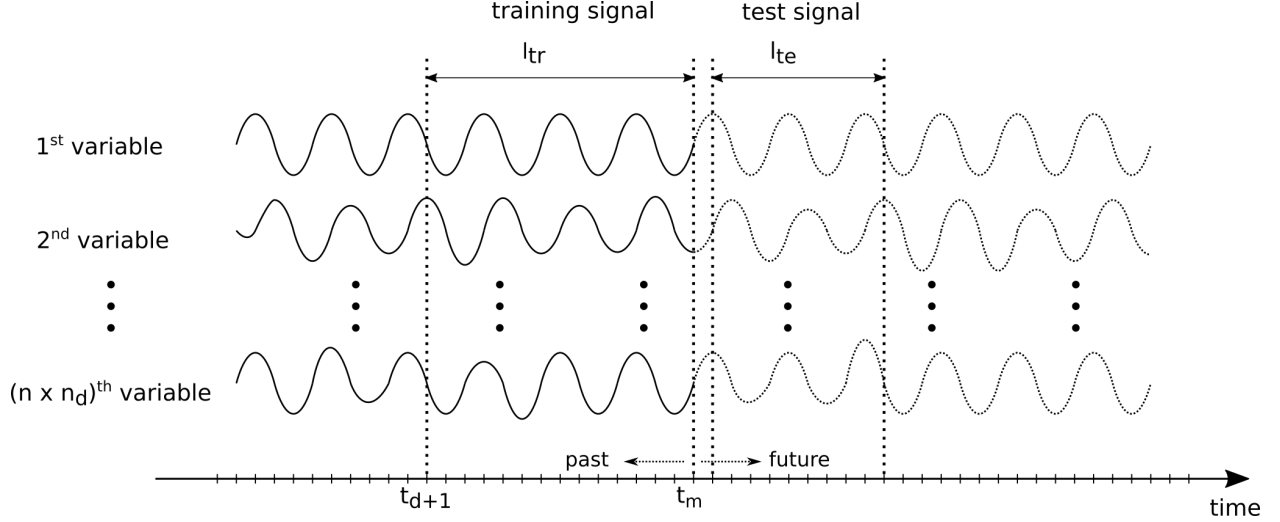


Figure 2: Sketch of the HDMD modeling approach.

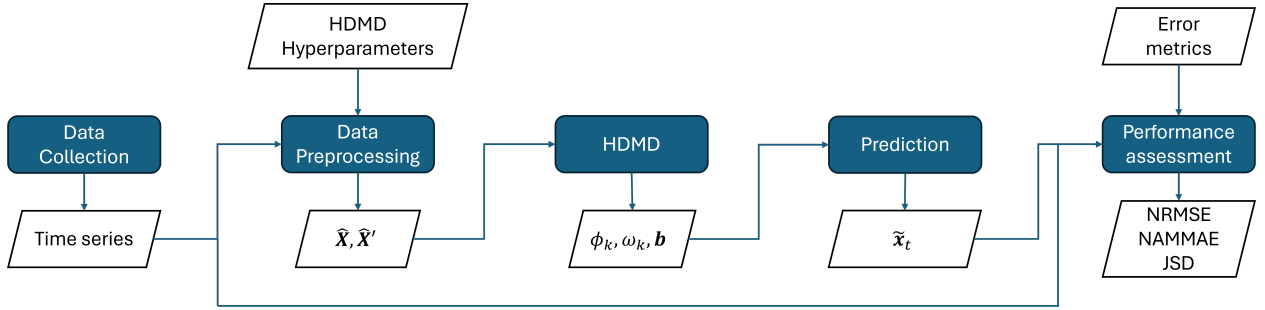


Figure 3: HDMD training-prediction-assessment flowchart

The DMD in its Hankel variation exposes two main hyperparameters concerning the length of the training time histories, l_{tr} , and the number of delayed copies expressed as the shift of the most delayed embedded time history l_d . Their values are an input of the preprocessing step, determining the organization of the time series data to obtain the correctly shaped Hankel matrices. The HDMD algorithm is thus applied, obtaining the eigenvalues and eigenvectors of the \mathbf{A} matrix, and the vector \mathbf{b} of the initial conditions. The forecasting analysis uses the output of the HDMD to calculate the predicted time series $\hat{\mathbf{x}}_t$ of the states, which are then compared with the test signals in order to evaluate the error metrics used to assess the algorithm performances.

A full-factorial numerical experiment is conducted to investigate the influence of the two main hyperparameters of the HDMD using 5 levels of variation for $l_{tr} = \hat{T}, 2\hat{T}, 4\hat{T}, 8\hat{T}, 16\hat{T}$ and 6 for $l_d = 0.5\hat{T}, \hat{T}, 2\hat{T}, 4\hat{T}, 8\hat{T}, 16\hat{T}$, as resumed in Table 1 also in terms of training time steps n_{tr} and number of delayed time histories embedded n_d with the current time sampling.

Table 1: List of the settings tested for Hankel-DMD hyperparameters

l_{tr}	[-]	\hat{T}	$2\hat{T}$	$4\hat{T}$	$8\hat{T}$	$16\hat{T}$
l_d	[-]	$0.5\hat{T}$	\hat{T}	$2\hat{T}$	$4\hat{T}$	$8\hat{T}$
n_{tr}	[samples]	73	146	293	585	1170
n_d	[samples]	37	73	146	293	585

4 Results

This section discusses the DMD analysis of the system dynamics in terms of complex modal frequencies, modal participation, and most energetic modes, and assesses the results of the DMD-based forecasting method for the prediction of the state evolution.

4.1 Modal analysis

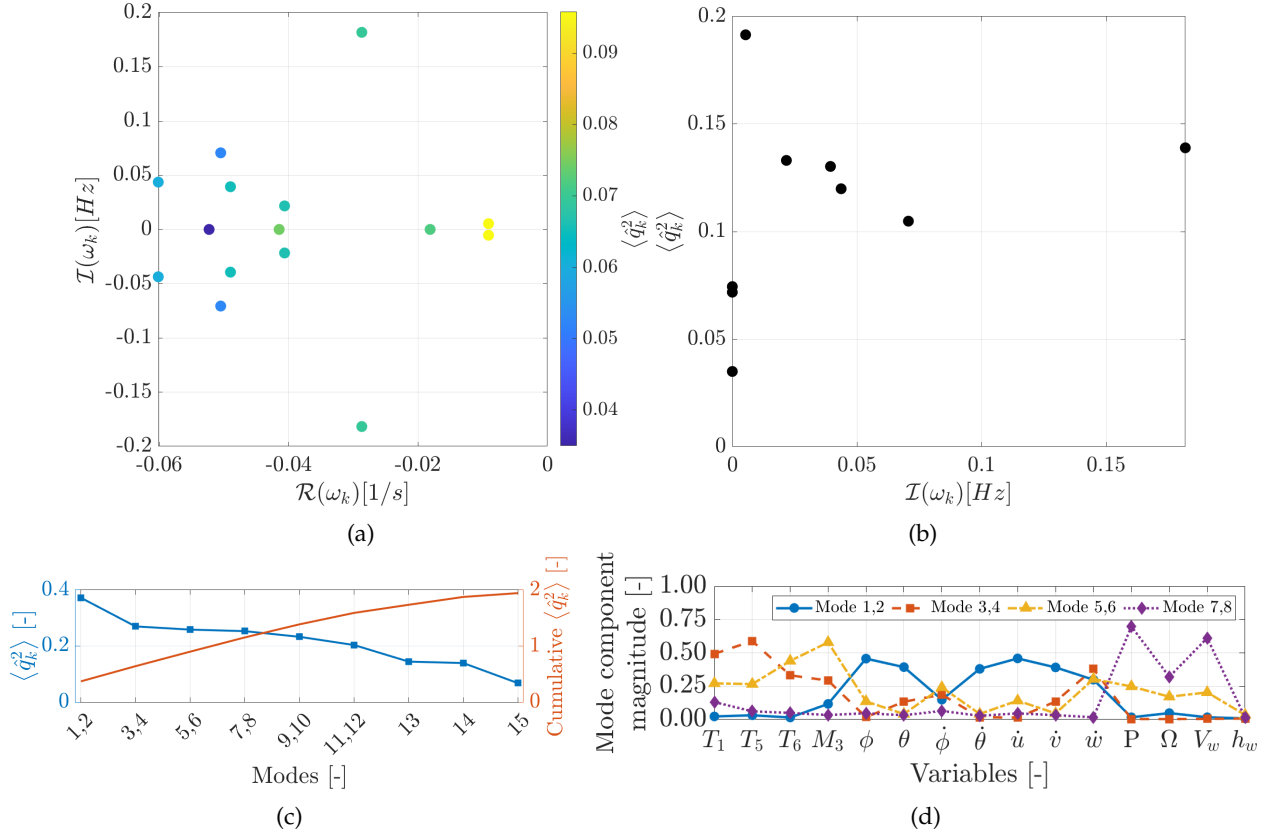


Figure 4: DMD complex modal frequencies, modal participation, and first modes for filtered z-scored data

Figure 4 shows the modal representation provided by the DMD for the current test case with standardized data with the application of the low-pass filter, with no state augmentation. Modes ϕ_k are ranked based on the energy of the respective modal coordinate signal normalized by the total energy

$$\langle \hat{q}_k^2 \rangle = \langle q_k^2 \rangle / \sum_k \langle q_k^2 \rangle. \quad (17)$$

Couples of complex conjugate modes and frequencies are grouped together in the analysis. The first four complex conjugate modes emerge as the most energetic as shown in Fig. 4c. Their shapes are reported in Fig. 4d. The variables' participation in the first mode (1,2) shows a significant coupling of pitch and roll motion, pitch angular rate, and accelerations along the three axes. It has a frequency of 0.0053 Hz corresponding to a long period of about 188 seconds. The second couple of modes (3,4) is characterized by a frequency of 0.1818 Hz, *i.e.*, a period of about 5.5 seconds, and show a strong coupling of forces acting on the tendons and the vertical acceleration of the floater (and, to a lower extent, of the y-axis acceleration and roll angular rate). The period of this mode is similar, yet shorter, to the average wave elevation period as identified from the spectrum of the relative signal. The third mode couple is the (5,6), dominated by the mooring and the tendons force (in particular tendon T_6), coupled with the roll angular rate, the vertical acceleration, and, more weakly, with the wind turbine extracted power, blades angular velocity, and wind

speed, showing a period of 46 seconds, and associated frequency of 0.0217 Hz. The wind turbine extracted power, blades angular velocity, and wind speed are the main actors in the last most energetic mode couple (7,8), characterized by a frequency of 0.0394 Hz, with a corresponding period of 25.37 seconds.

4.2 Forecasting via Hankel-DMD

In this work, the prediction of the system state involves applying a variant of the standard DMD algorithm, which uses a state augmentation strategy based on time-delayed copies of the state, called Hankel-DMD. As anticipated in Section 3, a full-factorial combination of parameter settings is tested to investigate the influence of the two main hyperparameters of the HDMD algorithm on its forecasting capability. The prediction performance of each configuration is assessed through the metrics introduced in Section 2.5 on a statistical basis using 250 random starting instants as test cases for prediction inside the 12-hour considered time frame.

A preliminary analysis concerns the effect on the prediction of the low-pass filtering preprocess. Three observation horizons are considered, using test signals l_{te} of length \hat{T} , $2\hat{T}$, and $4\hat{T}$. The results, gathering the outcomes from all the algorithm setups and test cases, are resumed in Fig. 5 as boxplots for the NRMSE, NAMMAE, and JSD. The boxplots show the first, second (equivalent to the median value), and third quartiles, while the whiskers extend from the box to the farthest data point lying within 1.5 times the inter-quartile range, defined as the difference between the third and the first quartiles from the box. Outliers are not shown to improve the readability of the plot. The filtering demonstrates helping the HDMD algorithm in

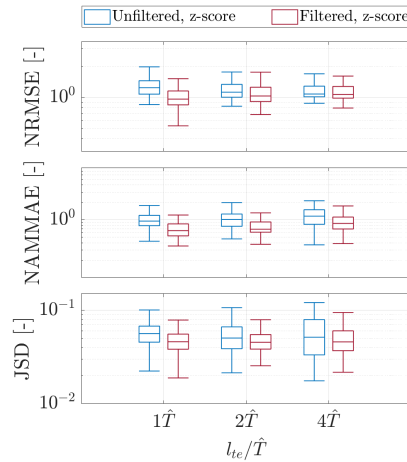


Figure 5: Influence of low-pass filtering on prediction performance of HDMD.

the prediction task, with a more pronounced effect in the short-term time window for all the performance metrics. This confirms the DMD suffering when applied to noisy datasets, as described in literature [8, 25].

The detailed analysis of the effect of the hyperparameters is thus carried on with the low-pass filtered data only. The obtained results are presented in Fig. 6 in terms of boxplots for the NRMSE, NAMMAE, and JSD evaluated focusing on a length of the test signal l_{te} of \hat{T} , $2\hat{T}$ and $4\hat{T}$. It can be noted that the three metrics indicate different *best* hyperparameter settings. However, the different types of errors targeted by the three metrics help to interpret the results and gain some insight:

- a) Long training signals with few delayed signals in the augmented state show poor prediction capabilities, as confirmed by all the metrics for both the short-term and mid-term time windows. The effect is notable for $\frac{l_d}{l_{tr}} < 1/8$.
- b) A high number of embedded time-delayed signals with insufficiently long training lengths is prone to produce NRMSE progressively reducing its dispersion around the value of 1 for longer observation windows. This happens, with the explored values of l_d , particularly for $l_{tr} = \hat{T}$, $2\hat{T}$, and, to a less extent, $4\hat{T}$, when $\frac{l_d}{l_{tr}}$ exceeds 1. At the same time, the NAMMAE and JSD values for the same settings are progressively increasing their values; this indicates that the predicted signals aren't able to catch the maximum and minimum values of the reference sequences when these appear to

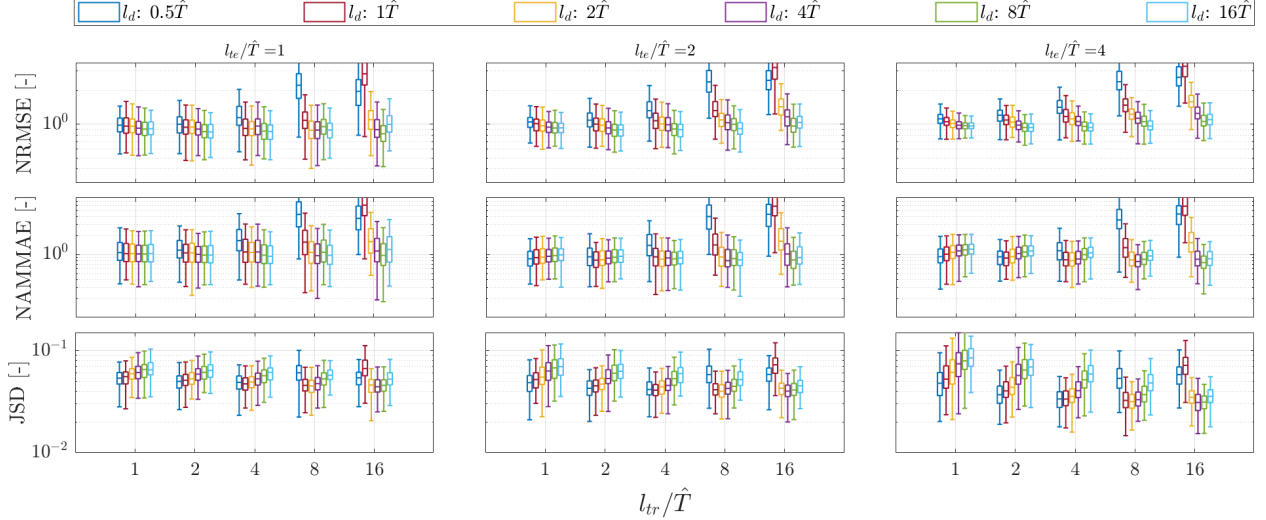


Figure 6: Filtered z-score data prediction, error metrics for $l_{te}/\hat{T} = 1$ (left column), 1 (center column), and 4 (right column).

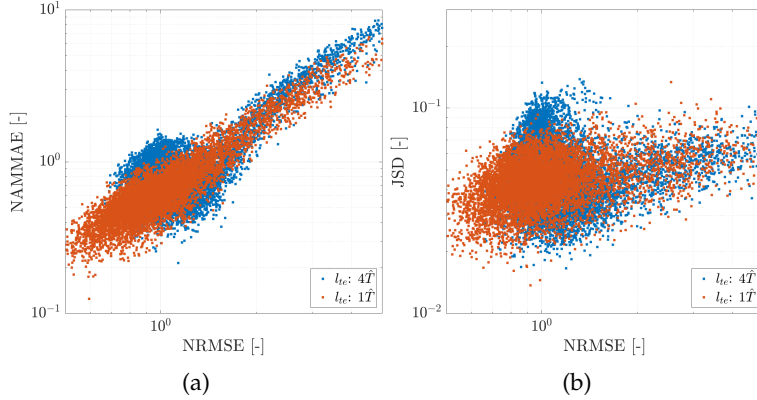


Figure 7: Correlation between metrics for $l_{te} = \hat{T}$ and $l_{te} = 4\hat{T}$

be not at the very beginning of the time histories and that the distribution of the predicted data is progressively losing adherence to the true data advancing in time. The combination of those two behaviors is due to the generation of a high number of rapidly decaying predictions, which signals become null after a short observation time. The analysis of the correlation between the error indices confirms the statement, see Fig. 7: for the longer observation period $l_{te} = 4\hat{T}$, several output sequences move to higher NAMMAE/JSD and NRMSE close to 1.

A suitable range for the hyperparameter settings can be inferred by combining the above considerations. The best results are obtained when $4 \leq l_{tr}/\hat{T} \leq 16$ and $\frac{1}{8} < l_d/l_{tr} < 1$. The forecast by the HDMD for a random test sequence is given in Fig. 8 as a representative prediction example. Results for other test cases can be found in the Supplementary Information. The forecasts are obtained using the hyperparameter settings in the middle of the identified *recommended* range, $l_{te} = 10\hat{T}$ and $l_d = 5.625\hat{T}$ ($n_d = 411$). The observed filtered (past) time histories are depicted in black, the predicted (future) time histories are in blue, and the true observed filtered (future) time histories are presented with a dashed black line; the unfiltered observed time histories, past and future, are in grey, solid and dashed respectively. In the first half of an incoming wave period, all the variables show a very good agreement between the predicted and the test signals. The adherence of the forecasts to the truth is good for most of the variables up to one period and in several test cases up to two periods. This forecasting time window can be assumed satisfactory from the perspective of the design of a model predictive or feedforward controller according to [40], where a five-second horizon is considered and found to be sufficient.

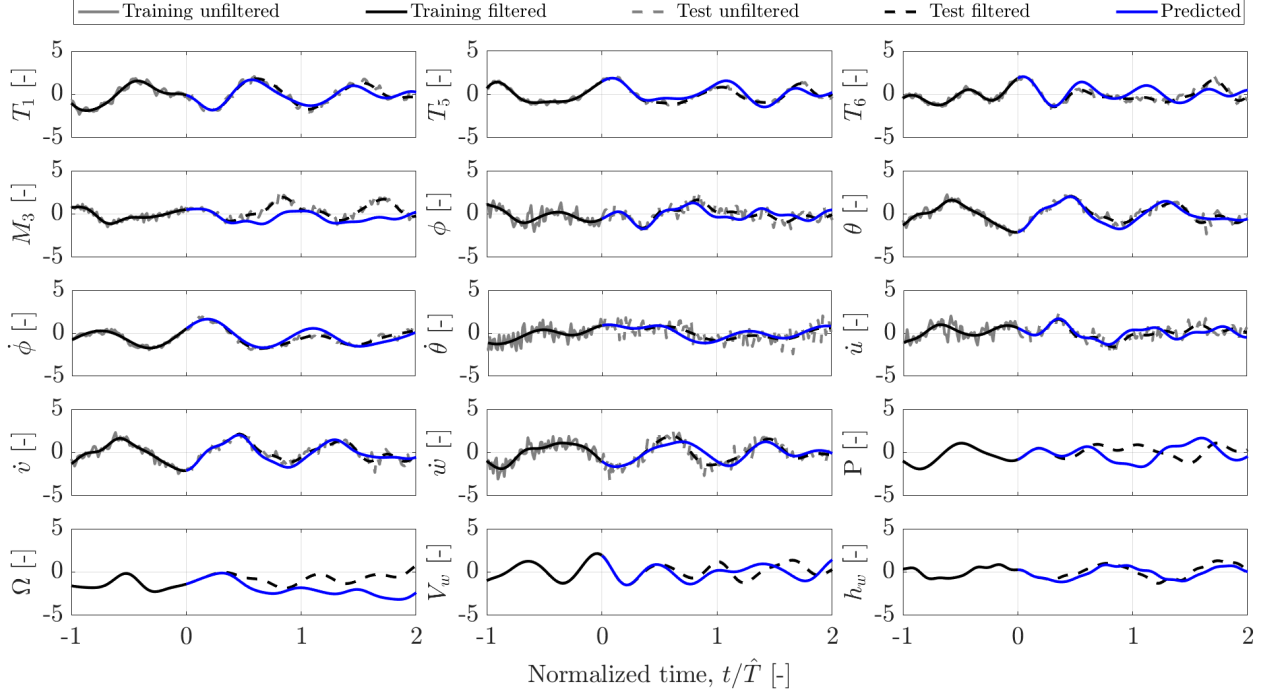


Figure 8: Time series prediction by HDMD, random test sequence.

The worst predicted variables are typically the wind speed estimated by the PLC on the nacelle, the power extracted by the wind turbine, and the rotational speed of its blades. The three are naturally correlated, with the wind speed being characterized by the largest stochasticity among all the variables under analysis. The other two variables in the mentioned subgroup are characterized by a strongly nonlinear behavior in the given dataset: the strong wind causes the power and the blades' rotational speed to be limited in their maximum values by the turbine control algorithms, which act as a saturator for such signals. In addition, and partially as a consequence of the above, these variables are seen to form an almost separate subsystem in the modal analysis of the given dataset; hence, a limited portion of the data can be actually used by the DMD to extract related modal content and produce their forecast, posing the method in a very challenging situation. Some difficulties are also encountered for the wave elevation. A possible explanation can be sought recalling that the corresponding sensor is physically separated from the platform; the ADCP measures the wave elevation 60 meters away from the platform, desynchronizing the information of this signal to the others. This is a probable cause for the modal analysis showing almost no participation of the variable h_w in all the modes but the less energetic one. Again, this makes the wave elevation a separate subsystem to be predicted by the DMD with a small subset of data.

4.3 Forecasting via Stochastic Hankel-DMD

A Stochastic extension of the Hankel-DMD (SHDMD) is obtained for floating wind turbine motion forecasting using experimental data, combining the insights gained on the hyperparameters' role during the deterministic analysis. A probabilistic length of the training time history is considered, uniformly distributed from 4 to 16 incoming wave periods, $l_{tr}/\hat{T} \sim \mathcal{U}(4, 16)$. Moreover, for each realization of l_{tr} , l_d is also taken as a probabilistic variable, uniformly distributed in the interval $l_d \sim \mathcal{U}\left(\frac{l_{tr}}{8}, l_{tr}\right)$ (each actual n_d is taken as its respective integer part). Figure 9 shows the results obtained using 100 uniformly distributed Monte Carlo realizations for the same test sequence of Fig. 8. The Supplementary Information contains the prediction for other random test cases presented for both the deterministic and stochastic analysis.

The observed filtered (past) time histories are depicted in black, the predicted (future) time histories are in blue, and the true observed filtered (future) time histories are presented with a dashed black line; the

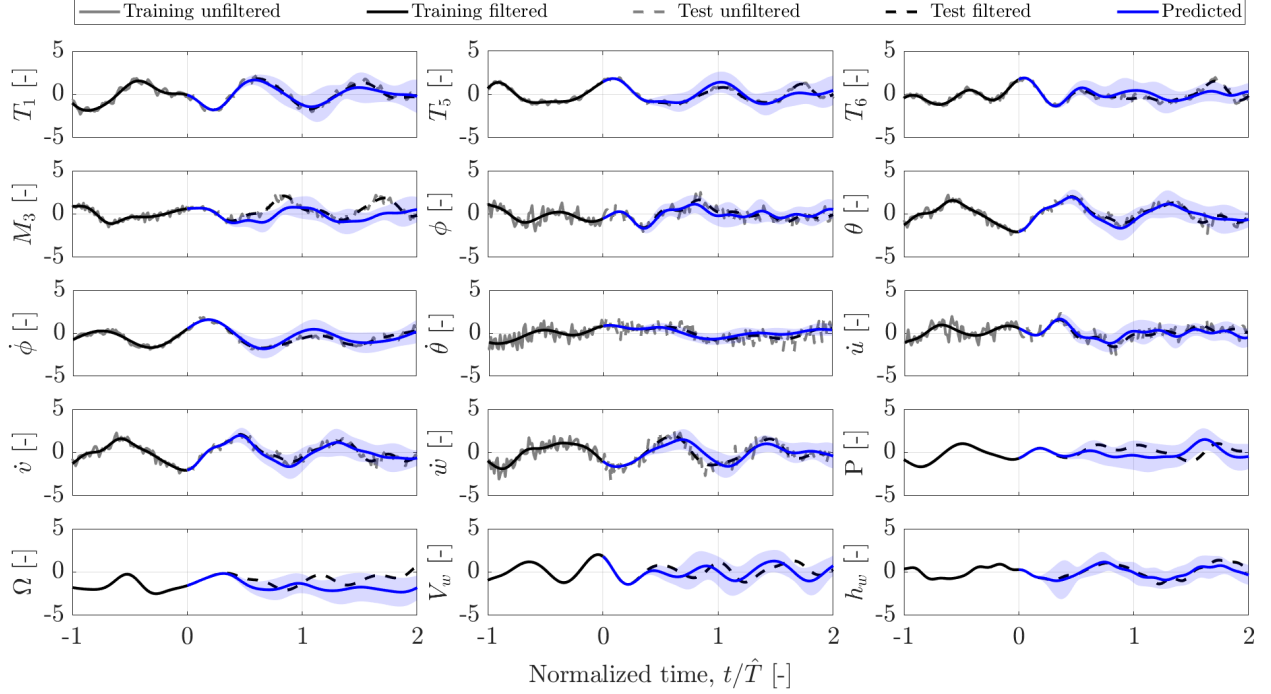


Figure 9: Time series prediction by SHDMD, random predicted sequence

unfiltered observed time histories, past and future, are in grey, solid and dashed respectively. Chebyshev's inequality is used for the shaded area, with a coverage factor equal to 2 (75% confidence interval).

The biggest discrepancies are noted, as for the deterministic case, in the prediction of P , Ω , and V_w , for which the predicted time histories faithfully reproduce the true data only for very short prediction windows, about a half of a wave encounter period long. For the other variables, the SHDMD provides good predictions of their time evolution, especially within the first wave encounter period. The performance is still fair for two wave encounter periods. It may be noticed how the reference curve (truth) almost always falls within the prediction uncertainty band.

Figure 10 compares the results of the stochastic and deterministic predictions for $l_{te}/\hat{T} = 1, 2$ and 4. For the stochastic case, the mean prediction is considered for the metrics evaluation. The stochastic approach is found to improve the prediction performance of the method, producing lower values for all the error metrics and both the observation lengths; the improvement is strongest for the shortest observation window, while the performances of the deterministic and stochastic approach tend to become similar for longer test periods.

It shall be noted that the evaluation time for a single DMD *training*, borrowing the term to make a parallelism with machine learning techniques, ranges from 0.001 s to 0.7 s on a mid-end laptop with an Intel Core i5-1235U CPU and 16Gb of memory using a non-compiled MATLAB code, depending on the algorithm setup (longer training signals with more delays require more time). The one-shot and computationally inexpensive training phase, related to direct linear algebra operations as detailed in Section 2.2, makes the HDMD and SHDMD algorithms very promising in the context of real-time forecasting and nowcasting. Moreover, the DMD and its variants are inherently suitable for continuous learning from an evolving changing system and environment, adapting the system identification and predictions along with the incoming data, making them promising tools also for the development of digital twins.

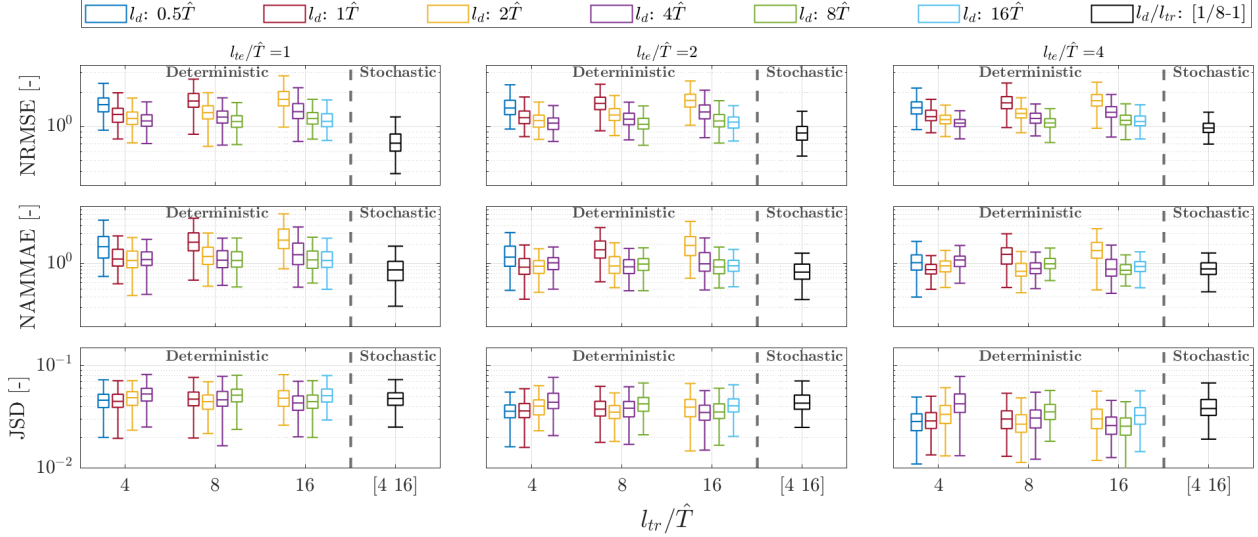


Figure 10: Error metrics for HDMD vs. SHDMD; $l_{te} = 1\hat{T}$ (left column), $l_{te} = 2\hat{T}$ (center column), and $l_{te} = 4\hat{T}$ (right column).

5 Conclusions

The dynamic mode decomposition (DMD) is applied to the measured data collected from an experimental floating wind turbine prototype installed offshore the Naples harbor, to perform system identification and forecasting.

The modal analysis shows that more than 50% of the total energy of the signals is represented by four modes. The most energetic mode is mostly participated by the components associated with floater accelerations, pitch and roll motion, and pitch rate; the second mode shows a strong coupling between the forces acting on the tendons and the vertical acceleration of the floater, with an oscillation period slightly shorter than the wave elevation period. Interestingly, the wind turbine extracted power and rpm and wind speed are almost not involved in the first two modes, result coupled as expected with the tendon and mooring tensions in the third mode, and are the main actors in the fourth mode.

The data-driven forecasting with the DMD in its Hankel version (HDMD) is assessed, investigating the effect of the algorithm hyperparameters (the length of the training time series and the number of delayed copies embedded in the augmented state) on its prediction capabilities. A full-factorial combination of parameter settings has been tested against 250 random test sequences. Three performance metrics are identified to control different aspects of the predicted time series: the NRMSE, the NAMMAE, and the JSD.

The proposed method is applied to predict quantities of interest for the FOWT that present a certain amount of predictably oscillatory behavior, but that are also subject to perturbations of stochastic and chaotic nature and subject to measuring noise. Separating the two components is not readily doable, posing a challenge for the DMD algorithm, typically well-performing on quasiperiodic systems. However, the HDMD demonstrated the capability of producing predictions with good agreement with the test signal in both the short- and medium-term.

An optimal setup does not emerge clearly from the numerical results. However, observing the values and trends of the three metrics, some indications about functional ranges for the hyperparameters' values are extracted.

A stochastic extension of the Hankel-DMD (SHDMD) is obtained using a probabilistic length of the training signals and number of embedded delayed time histories, providing a mean prediction with an associated uncertainty band. The interval of variation of the two hyperparameters is bounded following the insight gained from the full factorial analysis. The stochastic version of the algorithm was demonstrated to outperform the deterministic predictions in a statistical sense, with particular emphasis on shorter observation time windows.

A systematic difficulty is encountered in predicting a subset of variables which are found to form an almost independent subsystem from the modal analysis and expose the most nonlinear behavior in the extreme wind conditions registered in the used dataset. This constitutes an adverse situation for the DMD-based methods for forecasting, such that the effective prediction length for these variables is reduced to about half of a wave encounter period. Nevertheless, according to the literature, the time window in which the predictions stay accurate can be stated as satisfactory for the design and use of model predictive or feedforward controllers.

Concluding, the use of DMD-based algorithms to forecast the motions of a FOWT platform and other relevant quantities is an extremely promising method, particularly for short-term horizons. The peculiarities of the DMD make it suitable for real-time predictions, and able to continuously learn the ongoing evolution of the system characteristics. The mentioned abilities are crucial for advanced control applications, such as feedforward and model predictive controls which require a fast and accurate prediction algorithm to be integrated with, and digital twins applications both key enablers for further advancement in increased and stable power production from FOWT.

Acknowledgements

This research is supported by the Italian Ministry of the Environment and Energy Security (Ministero dell'Ambiente e della Sicurezza Energetica, MASE) through the Three-Year Plan for Electric System Research (Piano Triennale Ricerca di Sistema Elettrico) 2022-2024.

References

- [1] M. Al, A. Fontanella, D. van der Hoek, Y. Liu, M. Belloli, and J. W. van Wingerden. Feedforward control for wave disturbance rejection on floating offshore wind turbines. *Journal of Physics: Conference Series*, 1618(2):022048, sep 2020.
- [2] Ali Awada, Rafic Younes, and Adrian Ilinca. Review of vibration control methods for wind turbines. *Energies*, 14(11), 2021.
- [3] Tore Bakka and Hamid Karimi. Robust \mathcal{H}_∞ dynamic output feedback control synthesis with pole placement constraints for offshore wind turbine systems. *Mathematical Problems in Engineering*, 2012, 11 2012.
- [4] Mohammad Barooni and Deniz Velioglu Sogut. Forecasting pitch response of floating offshore wind turbines with a deep learning model. *Clean Technologies*, 6(2):418–431, 2024.
- [5] G. Betti, M. Farina, A. Marzorati, R. Scattolini, and G. A. Guagliardi. Modeling and control of a floating wind turbine with spar buoy platform. In *2012 IEEE International Energy Conference and Exhibition (ENERGYCON)*, pages 189–194, 2012.
- [6] Bingni W. Brunton, Lise A. Johnson, Jeffrey G. Ojemann, and J. Nathan Kutz. Extracting spatial-temporal coherent patterns in large-scale neural recordings using dynamic mode decomposition. *Journal of Neuroscience Methods*, 258:1–15, 2016.
- [7] Steven L. Brunton, Bingni W. Brunton, Joshua L. Proctor, Eurika Kaiser, and J. Nathan Kutz. Chaos as an intermittently forced linear system. *Nature Communications*, 8(1):19, May 2017.
- [8] Steven L. Brunton, Marko Budišić, Eurika Kaiser, and J. Nathan Kutz. Modern koopman theory for dynamical systems. *SIAM Review*, 64(2):229–340, 2022.
- [9] Global Wind Energy Council. Global offshore wind report 2020. *GWEC: Brussels, Belgium*, 19:10–12, 2020.
- [10] Henrique Dias Machado de Azevedo, Alex Maurício Araújo, and Nadège Bouchonneau. A review of wind turbine bearing condition monitoring: State of the art and challenges. *Renewable and Sustainable Energy Reviews*, 56:368–379, 2016.
- [11] Matteo Diez, Mauro Gaggero, and Andrea Serani. Data-driven forecasting of ship motions in waves using machine learning and dynamic mode decomposition. *International Journal of Adaptive Control and Signal Processing*, n/a(n/a), 2024.

- [12] Matteo Diez, Andrea Serani, Emilio F. Campana, and Frederick Stern. Time-series forecasting of ships maneuvering in waves via dynamic mode decomposition. *Journal of Ocean Engineering and Marine Energy*, 8(4):471–478, Nov 2022.
- [13] Matteo Diez, Andrea Serani, Mauro Gaggero, and Emilio Fortunato Campana. Improving knowledge and forecasting of ship performance in waves via hybrid machine learning methods. In *34th Symposium on Naval Hydrodynamics Washington, DC, USA, June 26 - July 1, 2022, 2022*.
- [14] Hongyang Dong, Mohamed Edrah, Xiaowei Zhao, Maurizio Collu, Xue Xu, Abhinav K A, and Zi Lin. Model-free semi-active structural control of floating wind turbines. In *2020 Chinese Automation Congress (CAC)*, pages 4216–4220, 2020.
- [15] Fiona Dunne, Lucy Pao, Alan Wright, Bonnie Jonkman, and Neil Kelley. *Combining Standard Feedback Controllers with Feedforward Blade Pitch Control for Load Mitigation in Wind Turbines*.
- [16] Fiona Dunne, Lucy Pao, Alan Wright, Bonnie Jonkman, Neil Kelley, and Eric Simley. *Adding Feedforward Blade Pitch Control for Load Mitigation in Wind Turbines: Non-Causal Series Expansion, Preview Control, and Optimized FIR Filter Methods*.
- [17] Fiona Dunne, David Schlipf, Lucy Pao, Alan Wright, Bonnie Jonkman, Neil Kelley, and Eric Simley. *Comparison of Two Independent Lidar-Based Pitch Control Designs*.
- [18] Daniel Dylewsky, David Barajas-Solano, Tong Ma, Alexandre M. Tartakovsky, and J. Nathan Kutz. Stochastically forced ensemble dynamic mode decomposition for forecasting and analysis of near-periodic systems. *IEEE Access*, 10:33440–33448, 2022.
- [19] Robert Falkner. The paris agreement and the new logic of international climate politics. *International Affairs*, 92(5):1107–1125, 2016.
- [20] Mihai Florian and John Dalsgaard Sørensen. Wind turbine blade life-time assessment model for preventive planning of operation and maintenance. *Journal of Marine Science and Engineering*, 3(3):1027–1040, 2015.
- [21] A. Fontanella, M. Al, J.-W. van Wingerden, and M. Belloli. Model-based design of a wave-feedforward control strategy in floating wind turbines. *Wind Energy Science*, 6(3):885–901, 2021.
- [22] J Galván, M J Sánchez-Lara, I Mendikoa, G Pérez-Morán, V Nava, and R Rodríguez-Arias. Nautilus-tu10 mw floating offshore wind turbine at gulf of maine: Public numerical models of an actively ballasted semisubmersible. *Journal of Physics: Conference Series*, 1102(1):012015, oct 2018.
- [23] Elenya Grant, Kathryn Johnson, Rick Damiani, Mandar Phadnis, and Lucy Pao. Buoyancy can ballast control for increased power generation of a floating offshore wind turbine with a light-weight semi-submersible platform. *Applied Energy*, 330:120287, 2023.
- [24] M Harris, M Hand, and A Wright. Lidar for turbine control: March 1, 2005 - november 30, 2005. Technical report, NREL - National Wind Technology Center, 1 2006.
- [25] Maziar S. Hemati, Clarence W. Rowley, Eric A. Deem, and Louis N. Cattafesta. De-biasing the dynamic mode decomposition for applied koopman spectral analysis of noisy datasets. *Theoretical and Computational Fluid Dynamics*, 31(4):349–368, Aug 2017.
- [26] International Energy Agency (IEA). Net zero by 2050, 2021. Paris.
- [27] Jason Jonkman. Dynamics modeling and loads analysis of an offshore floating wind turbine, 2007.
- [28] Jason Jonkman. Influence of control on the pitch damping of a floating wind turbine. In *46th AIAA Aerospace Sciences Meeting and Exhibit*, 2008.
- [29] Mason Kamb, Eurika Kaiser, Steven L. Brunton, and J. Nathan Kutz. Time-delay observables for koopman: Theory and applications. *SIAM Journal on Applied Dynamical Systems*, 19(2):886–917, 2020.
- [30] A. A. Kaptanoglu, K. D. Morgan, C. J. Hansen, and S. L. Brunton. Characterizing magnetized plasmas with dynamic mode decomposition. *Physics of Plasmas*, 27(3):032108, 03 2020.
- [31] E I Konstantinidis and P N Botsaris. Wind turbines: current status, obstacles, trends and technologies. *IOP Conference Series: Materials Science and Engineering*, 161(1):012079, nov 2016.
- [32] S. Kullback and R. A. Leibler. On information and sufficiency. *The Annals of Mathematical Statistics*, 22(1):79–86, 1951.
- [33] J. Kutz, Steven Brunton, Bingni Brunton, and Joshua Proctor. *Dynamic Mode Decomposition: Data-Driven Modeling of Complex Systems*. 11 2016.

- [34] Jason Laks, Lucy Pao, Alan Wright, Neil Kelley, and Bonnie Jonkman. *Blade Pitch Control with Preview Wind Measurements*.
- [35] T J Larsen and T D Hanson. A method to avoid negative damped low frequent tower vibrations for a floating, pitch controlled wind turbine. *Journal of Physics: Conference Series*, 75(1):012073, jul 2007.
- [36] Frank Lemmer (né Sandner), Wei Yu, David Schlipf, and Po Wen Cheng. Robust gain scheduling baseline controller for floating offshore wind turbines. *Wind Energy*, 23(1):17–30, 2020.
- [37] Xianwei Li and Huijun Gao. Load mitigation for a floating wind turbine via generalized h_∞ structural control. *IEEE Transactions on Industrial Electronics*, 63(1):332–342, 2016.
- [38] J. Lin. Divergence measures based on the shannon entropy. *IEEE Transactions on Information Theory*, 37(1):145–151, 1991.
- [39] Javier López-Queija, Eider Robles, Josu Jugo, and Santiago Alonso-Quesada. Review of control technologies for floating offshore wind turbines. *Renewable and Sustainable Energy Reviews*, 167:112787, 2022.
- [40] Yu Ma, Paul D. Sclavounos, John Cross-Whiter, and Dhiraj Arora. Wave forecast and its application to the optimal control of offshore floating wind turbine for load mitigation. *Renewable Energy*, 128:163–176, 2018.
- [41] Jordan Mann and J. Nathan Kutz. Dynamic mode decomposition for financial trading strategies. *Quantitative Finance*, 16(11):1643–1655, 2016.
- [42] Kyle E. Marlantes, Piotr J. Bandyk, and Kevin J. Maki. Predicting ship responses in different seaways using a generalizable force correcting machine learning method. *Ocean Engineering*, 312:119110, 2024.
- [43] J. McMorland, M. Collu, D. McMillan, and J. Carroll. Operation and maintenance for floating wind turbines: A review. *Renewable and Sustainable Energy Reviews*, 163:112499, 2022.
- [44] Benedetto Nastasi, Natasa Markovska, Tomislav Puksec, Neven Duić, and Aoife Foley. Renewable and sustainable energy challenges to face for the achievement of sustainable development goals. *Renewable and Sustainable Energy Reviews*, 157:112071, 2022.
- [45] Manmathakrishnan Palraj and Panneerselvam Rajamanickam. Motion control studies of a barge mounted offshore dynamic wind turbine using gyrostabilizer. *Ocean Engineering*, 237:109578, 2021.
- [46] Shaowu Pan and Karthik Duraisamy. On the structure of time-delay embedding in linear models of non-linear dynamical systems. *Chaos: An Interdisciplinary Journal of Nonlinear Science*, 30(7):073135, 07 2020.
- [47] Gayathri Prakash, Harold Anuta, N Wagner, G Gallina, D Gielen, and R Gorini. Future of wind-deployment, investment, technology, grid integration and socio-economic aspects. *International Renewable Energy Agency (IRENA)*, 2019.
- [48] Joshua L. Proctor and Philip A. Eckhoff. Discovering dynamic patterns from infectious disease data using dynamic mode decomposition. *International Health*, 7(2):139–145, 02 2015.
- [49] L. Pustina, C. Lugni, G. Bernardini, J. Serafini, and M. Gennaretti. Control of power generated by a floating offshore wind turbine perturbed by sea waves. *Renewable and Sustainable Energy Reviews*, 132:109984, 2020.
- [50] L. Pustina, J. Serafini, C. Pasquali, L. Solero, A. Lidozzi, and M. Gennaretti. A novel resonant controller for sea-induced rotor blade vibratory loads reduction on floating offshore wind turbines. *Renewable and Sustainable Energy Reviews*, 173:113073, 2023.
- [51] Steffen Raach, David Schlipf, Frank Sandner, Denis Matha, and Po Wen Cheng. Nonlinear model predictive control of floating wind turbines with individual pitch control. In *2014 American Control Conference*, pages 4434–4439, 2014.
- [52] M. Rialti and G. Cimatti. *AEROGENERATORE mod. TN535 DESCRIZIONE GENERALE*. Tozzi Green, 2016.
- [53] Chan Roh. Deep-learning-based pitch controller for floating offshore wind turbine systems with compensation for delay of hydraulic actuators. *Energies*, 15(9), 2022.
- [54] CLARENCE W. ROWLEY, IGOR MEZIĆ, SHERVIN BAGHERI, PHILIPP SCHLATTER, and DAN S. HENNINGSON. Spectral analysis of nonlinear flows. *Journal of Fluid Mechanics*, 641:115–127, 2009.
- [55] CLARENCE W. ROWLEY, IGOR MEZIĆ, SHERVIN BAGHERI, PHILIPP SCHLATTER, and DAN S. HENNINGSON. Spectral analysis of nonlinear flows. *Journal of Fluid Mechanics*, 641:115–127, 2009.

- [56] Tom Salic, Jean Frédéric Charpentier, Mohamed Benbouzid, and Marc Le Boulluec. Control strategies for floating offshore wind turbine: Challenges and trends. *Electronics*, 8(10), 2019.
- [57] Saptarshi Sarkar, Breiffni Fitzgerald, and Biswajit Basu. Individual blade pitch control of floating offshore wind turbines for load mitigation and power regulation. *IEEE Transactions on Control Systems Technology*, 29(1):305–315, 2021.
- [58] David Schlipf, Eric Simley, Frank Lemmer, Lucy Pao, and Po Wen Cheng. Collective pitch feedforward control of floating wind turbines using lidar. *Journal of Ocean and Wind Energy*, 2, 11 2015.
- [59] PETER J. SCHMID. Dynamic mode decomposition of numerical and experimental data. *Journal of Fluid Mechanics*, 656:5–28, 2010.
- [60] Onofrio Semeraro, Gabriele Bellani, and Fredrik Lundell. Analysis of time-resolved piv measurements of a confined turbulent jet using pod and koopman modes. *Experiments in Fluids*, 53(5):1203–1220, Nov 2012.
- [61] A. Serani, M. Diez, S. Aram, D. Wundrow, D. Drazen, and K. McTaggart. Model order reduction of 5415m in irregular waves via dynamic mode decomposition: Computational models’ diagnostics, forecasting, and system identification capabilities. In *35th Symposium on Naval Hydrodynamics, Nantes, France, July 8th – 12th, 2024*.
- [62] Andrea Serani, Paolo Dragone, Frederick Stern, and Matteo Diez. On the use of dynamic mode decomposition for time-series forecasting of ships operating in waves. *Ocean Engineering*, 267:113235, 2023.
- [63] Yulin Si, Hamid Reza Karimi, and Huijun Gao. Modelling and optimization of a passive structural control design for a spar-type floating wind turbine. *Engineering Structures*, 69:168–182, 2014.
- [64] Eric Simley, Pietro Bortolotti, Andrew Scholbrock, David Schlipf, and Katherine Dykes. Iea wind task 32 and task 37: Optimizing wind turbines with lidar-assisted control using systems engineering. *Journal of Physics: Conference Series*, 1618(4):042029, sep 2020.
- [65] G. Song, F. Alizard, J.-C. Robinet, and X. Gloerfelt. Global and Koopman modes analysis of sound generation in mixing layers. *Physics of Fluids*, 25(12):124101, 12 2013.
- [66] ZhanQi Tang and Nan Jiang. Dynamic mode decomposition of hairpin vortices generated by a hemisphere protuberance. *Science China Physics, Mechanics and Astronomy*, 55(1):118–124, Jan 2012.
- [67] Edem Y. Tetteh, Kevin Fletcher, Chris Qin, Eric Loth, and Rick Damiani. Active ballasting actuation for the spiderfloat offshore wind turbine platform. In *AIAA SCITECH 2022 Forum*.
- [68] The European Parliament and Council. Directive (eu) 2018/2001 of the european parliament and of the council of 11 december 2018 on the promotion of the use of energy from renewable sources, 2018.
- [69] Ramji Tiwari and N. Ramesh Babu. Recent developments of control strategies for wind energy conversion system. *Renewable and Sustainable Energy Reviews*, 66:268–285, 2016.
- [70] Jonathan H. Tu, Clarence W. Rowley, Dirk M. Luchtenburg, Steven L. Brunton, and J. Nathan Kutz. On dynamic mode decomposition: Theory and applications. *Journal of Computational Dynamics*, 1(2):391–421, 2014.
- [71] Feng Yang, Qing-wang Song, Lei Wang, Shan Zuo, and Sheng-shan Li. Wind and wave disturbances compensation to floating offshore wind turbine using improved individual pitch control based on fuzzy control strategy. *Abstract and Applied Analysis*, 2014(1):968384, 2014.
- [72] Wei Yu, Frank Lemmer, David Schlipf, Po Wen Cheng, Bart Visser, Harmen Links, Neelabh Gupta, Sabrina Dankemann, Bernardino Counago, and Jose Serna. Evaluation of control methods for floating offshore wind turbines. *Journal of Physics: Conference Series*, 1104(1):012033, oct 2018.

Supplementary Information

Filtered data deterministic prediction - $\frac{l_{tr}}{\hat{T}} = 10 - \frac{l_d}{\hat{T}} = 5.625$

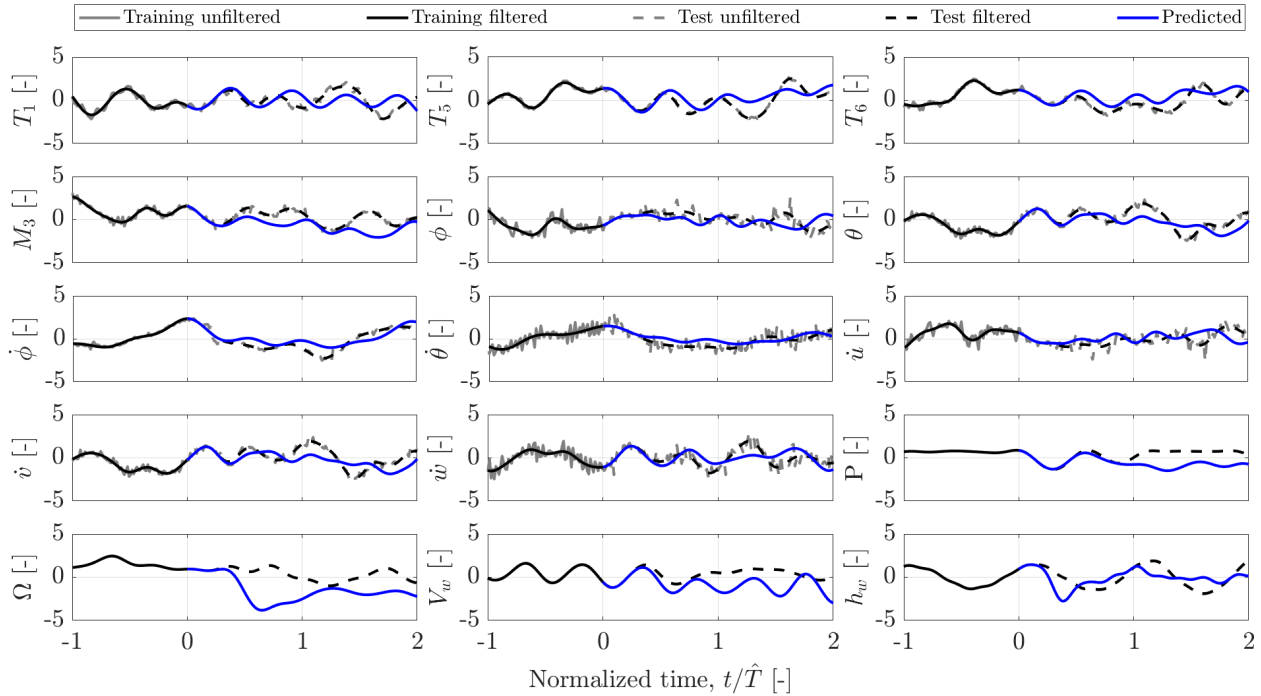


Figure 11: Filtered z-score data prediction, HDMD approach, random predicted sequence n.35

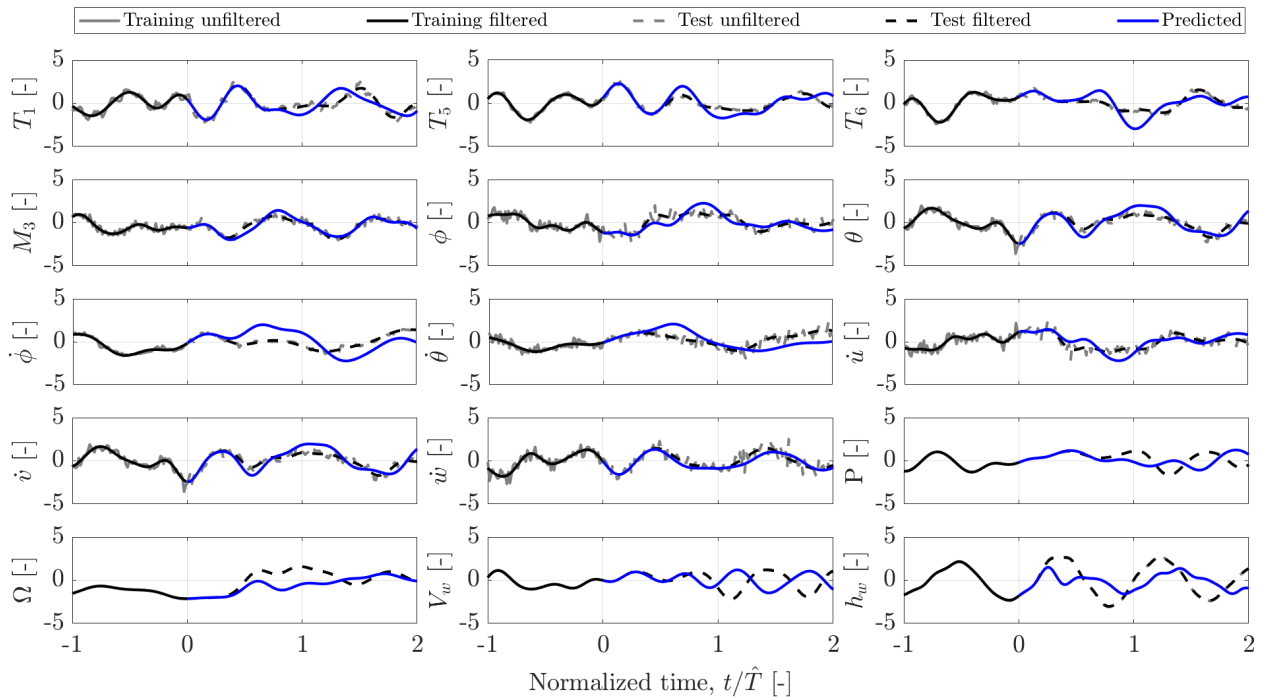


Figure 12: Filtered z-score data prediction, HDMD approach, random predicted sequence n.61

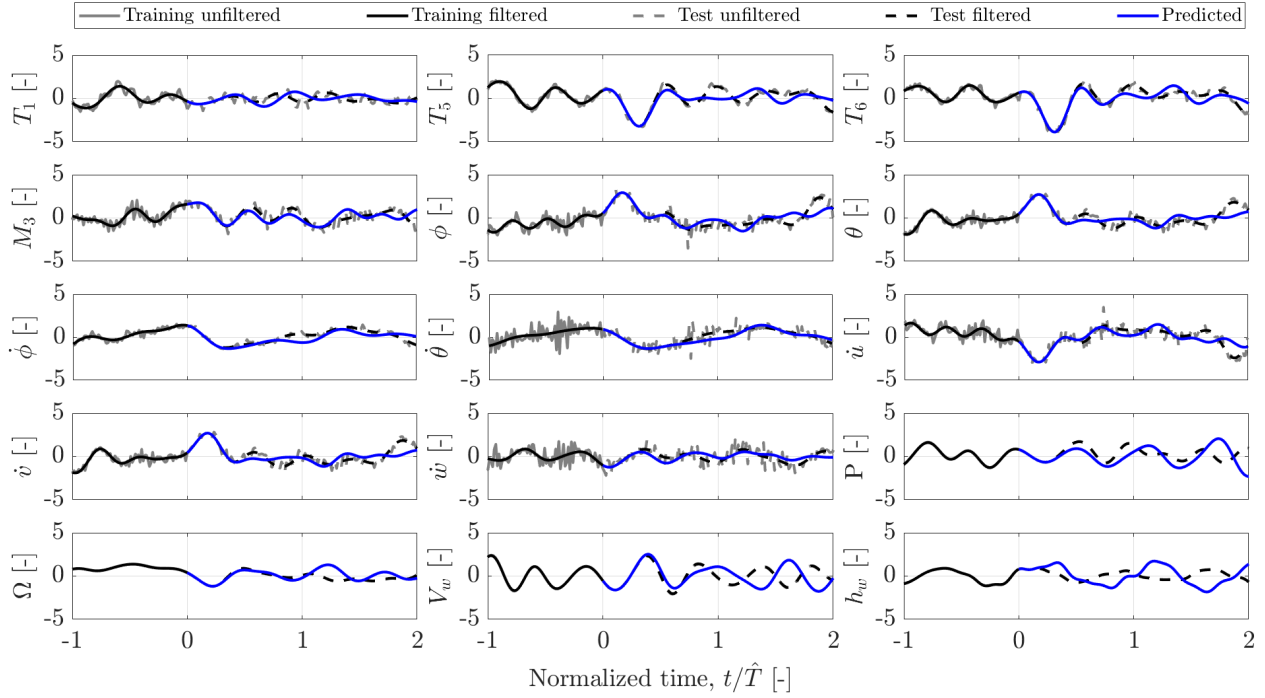


Figure 13: Filtered z-score data prediction, HDMD approach, random predicted sequence n.88

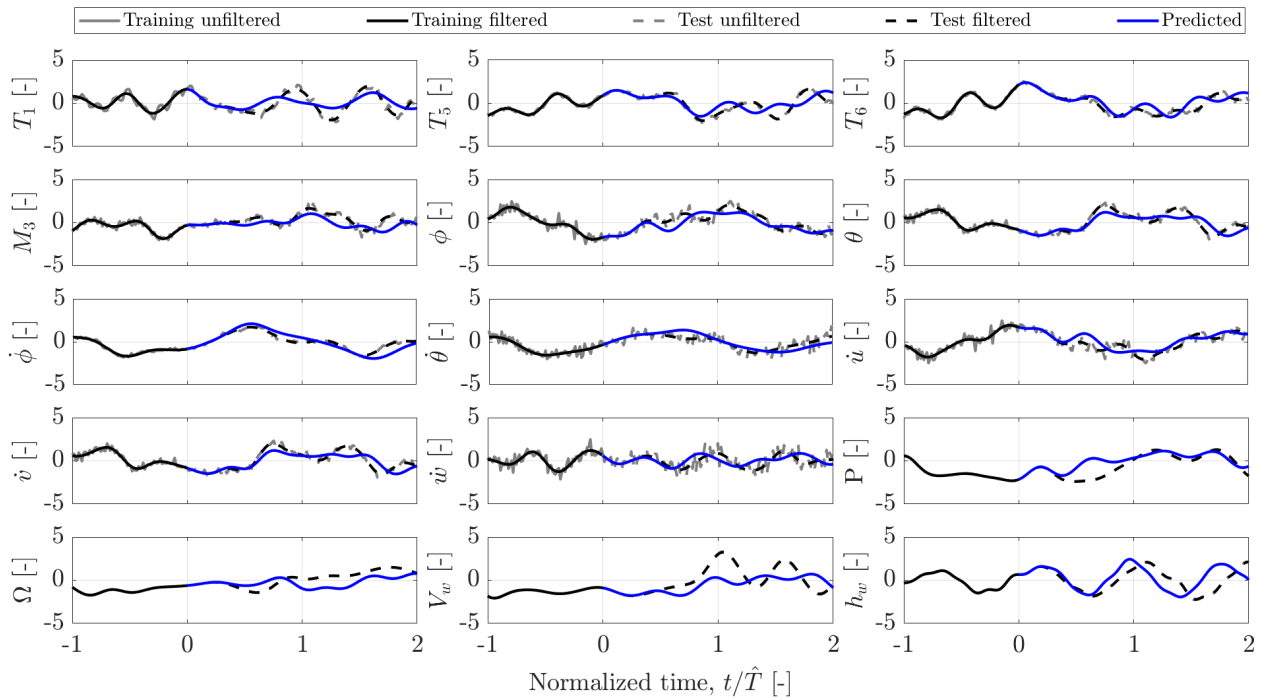


Figure 14: Filtered z-score data prediction, HDMD approach, random predicted sequence n.137

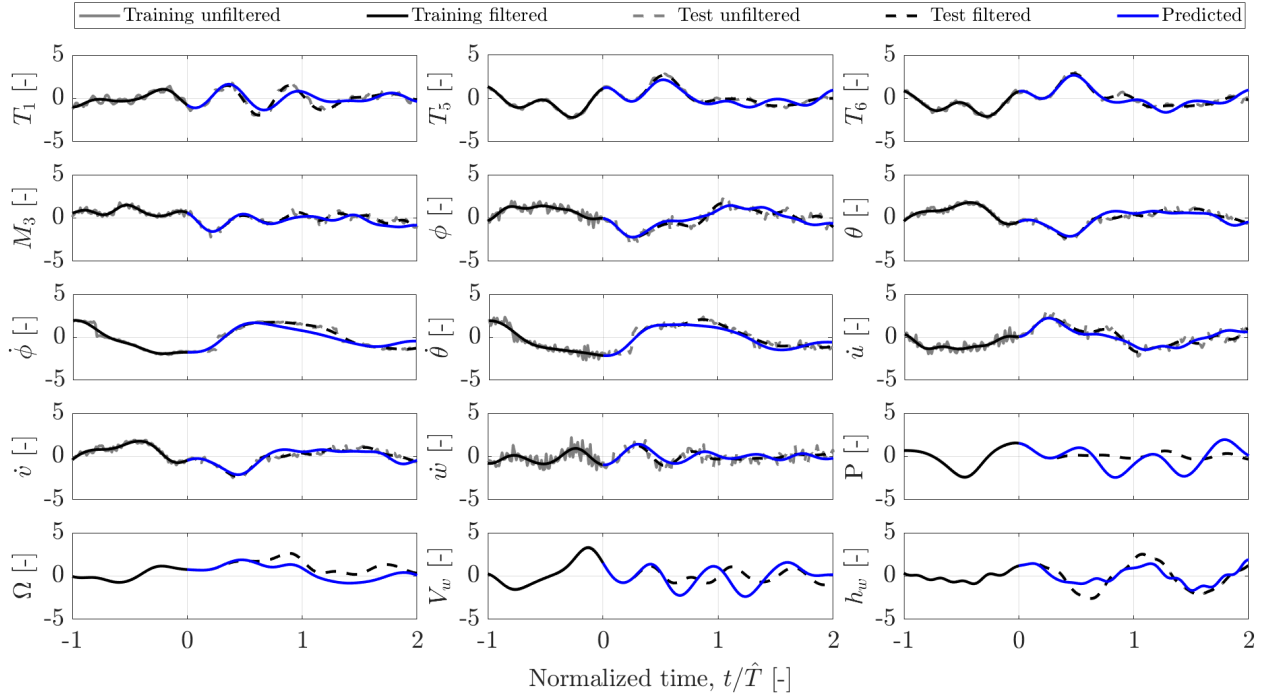


Figure 15: Filtered z-score data prediction, HDMD approach, random predicted sequence n.157

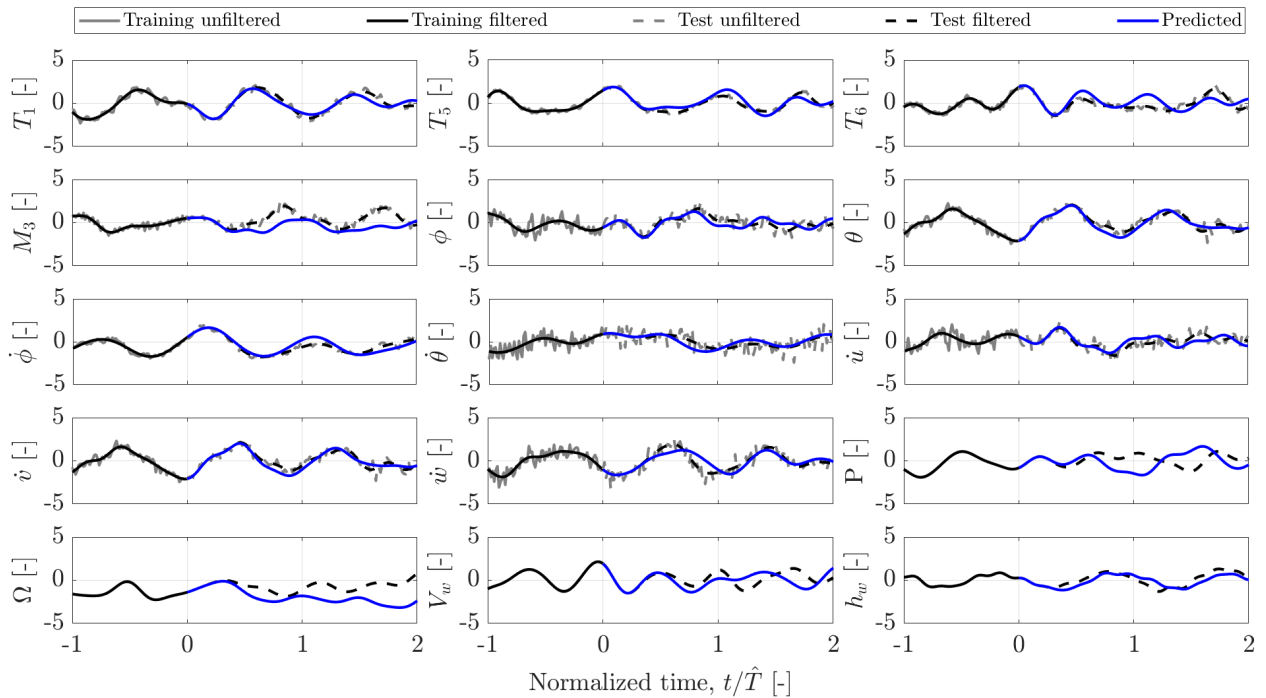


Figure 16: Filtered z-score data prediction, HDMD approach, random predicted sequence n.211

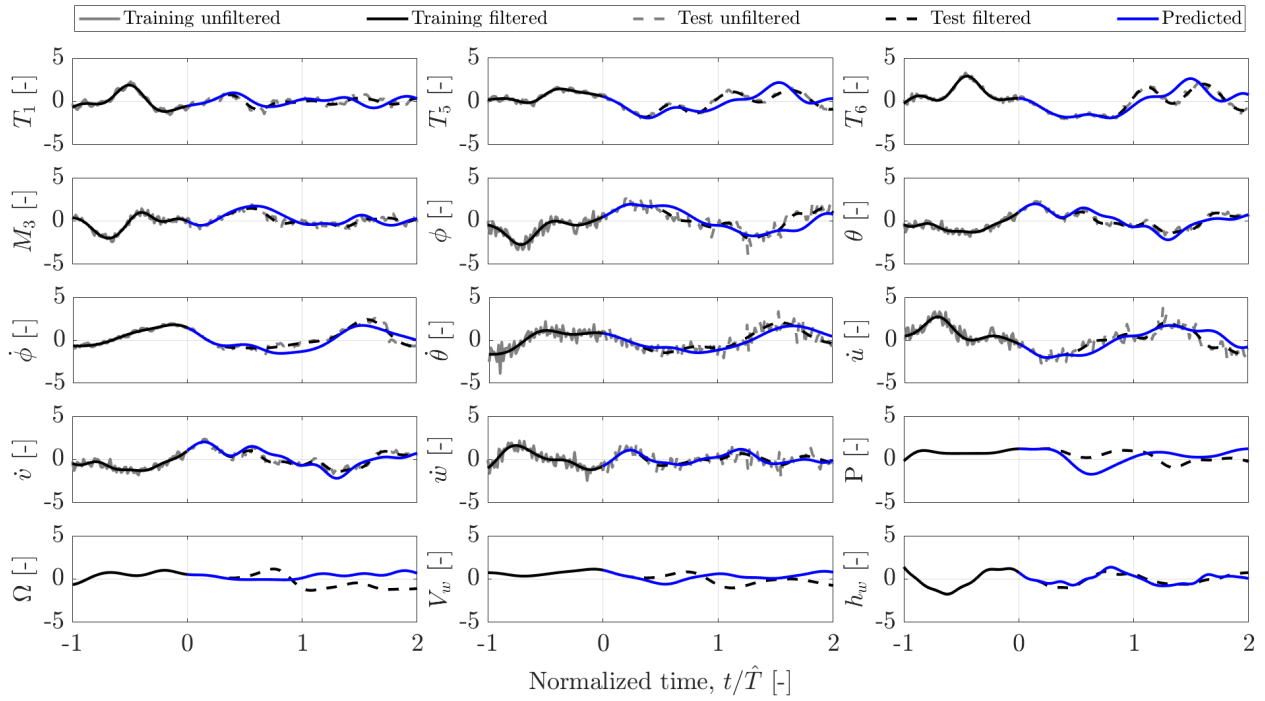


Figure 17: Filtered z-score data prediction, HDMD approach, random predicted sequence n.223

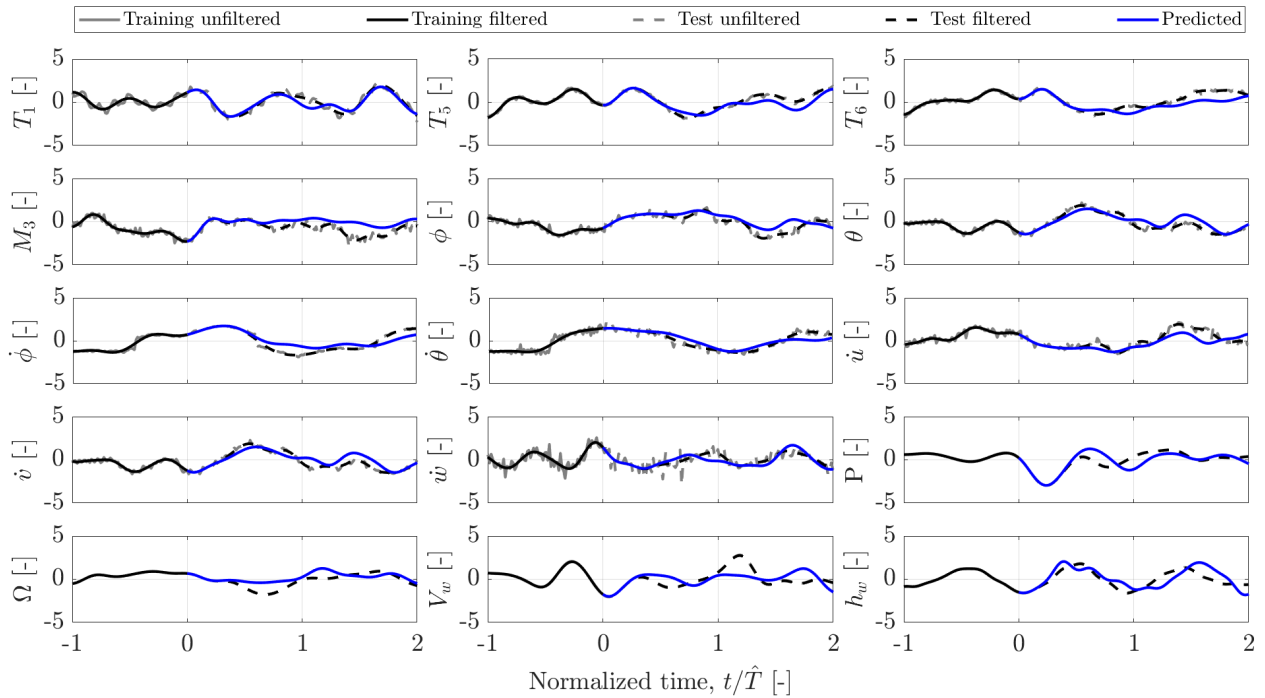


Figure 18: Filtered z-score data prediction, HDMD approach, random predicted sequence n.240

Filtered data stochastic prediction - $4 \leq \frac{l_{tr}}{\hat{T}} \leq 16$ - $\frac{1}{8} \leq \frac{l_d}{l_{tr}} \leq 1$

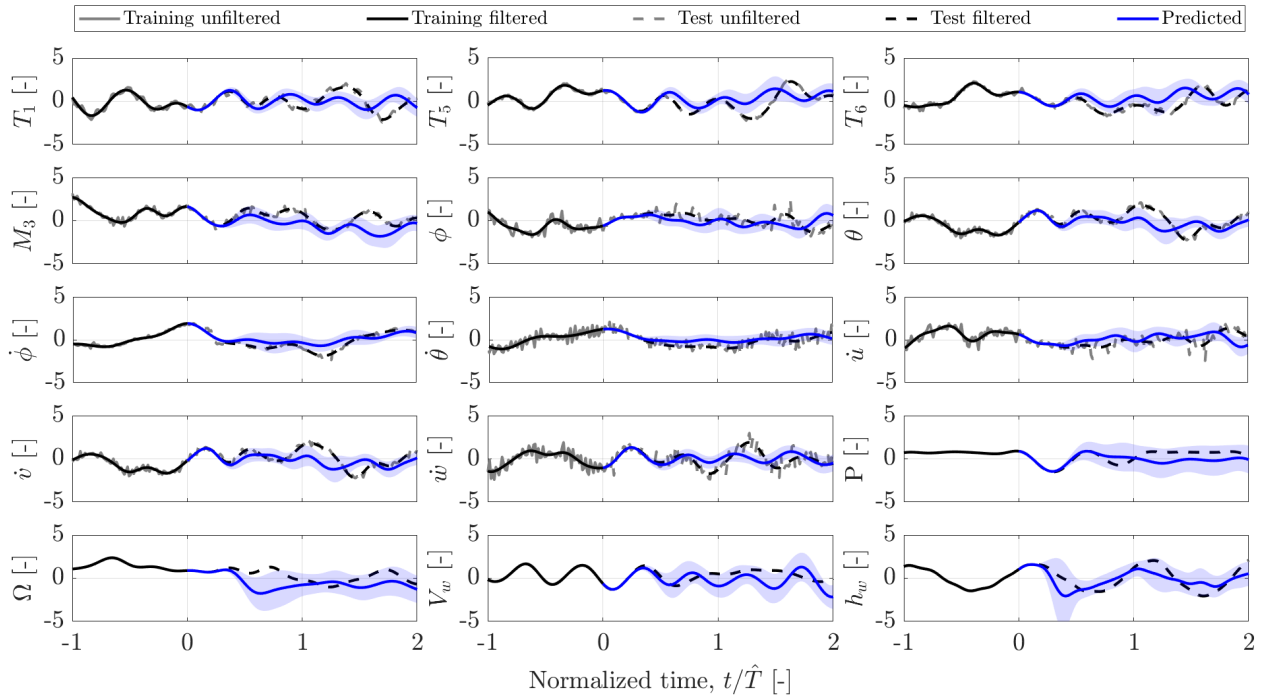


Figure 19: Filtered z-score data prediction, SHDMD approach, random predicted sequence n.35

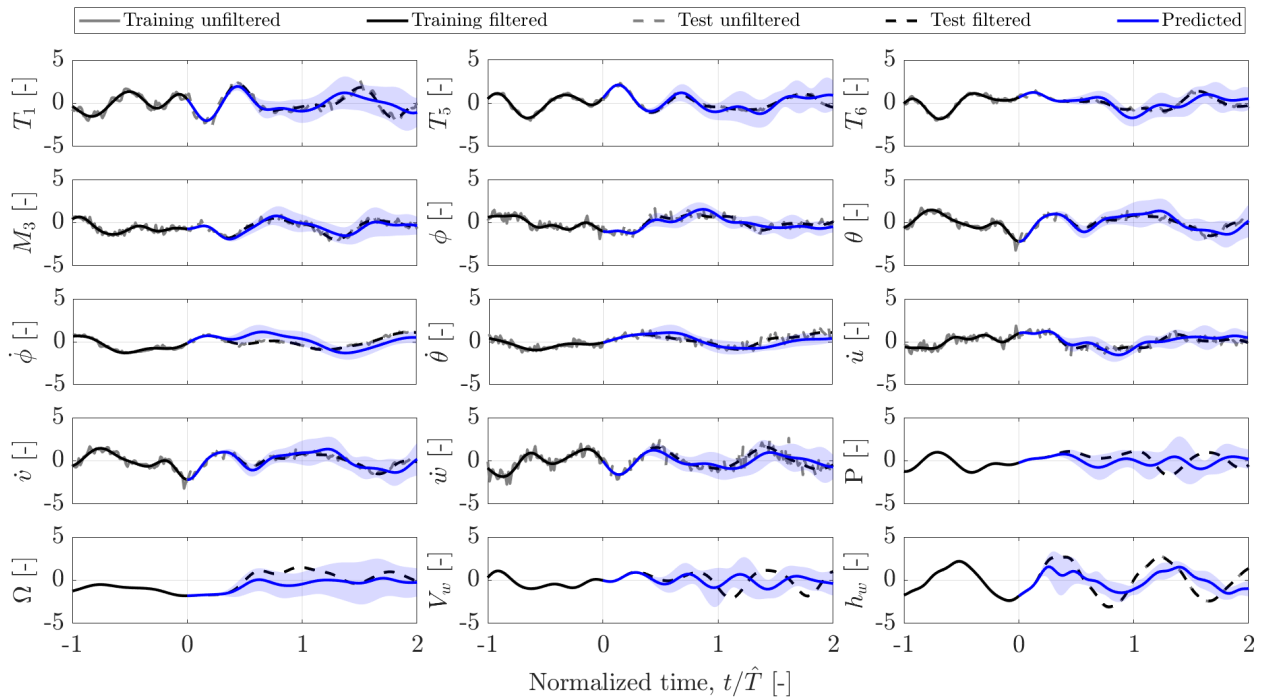


Figure 20: Filtered z-score data prediction, SHDMD approach, random predicted sequence n.61

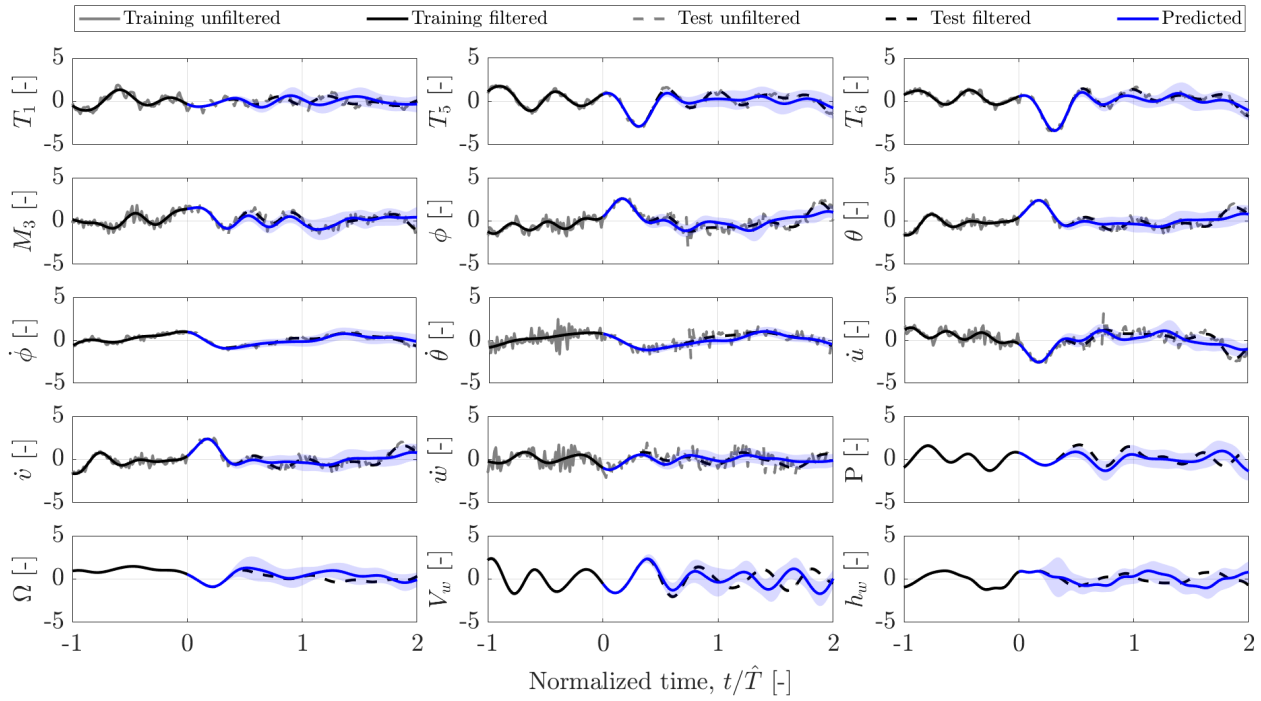


Figure 21: Filtered z-score data prediction, SHDMD approach, random predicted sequence n.88

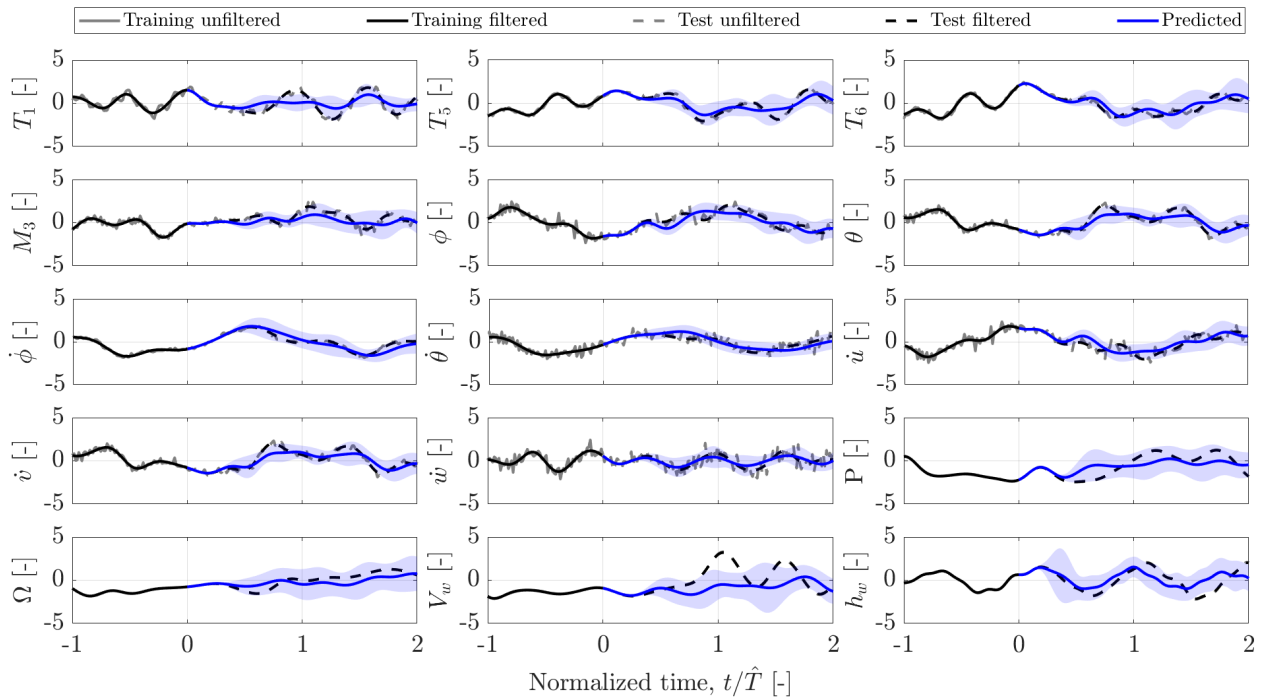


Figure 22: Filtered z-score data prediction, SHDMD approach, random predicted sequence n.137

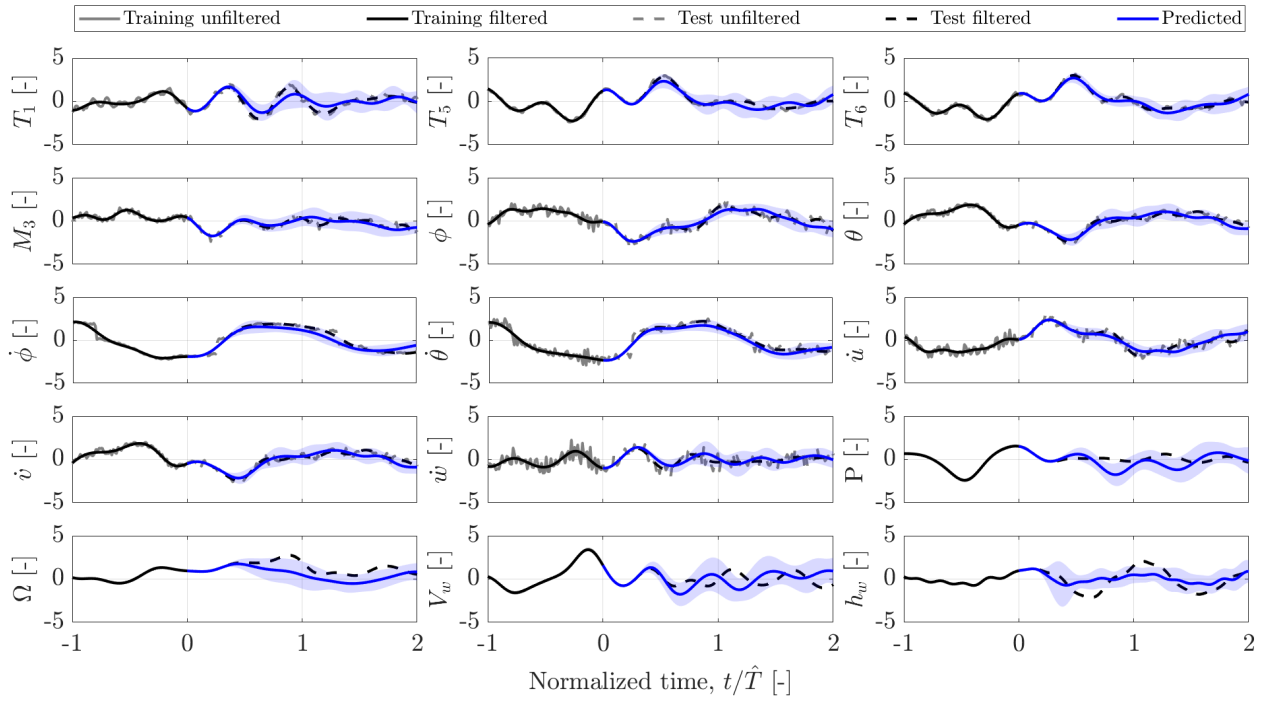


Figure 23: Filtered z-score data prediction, SHDMD approach, random predicted sequence n.157

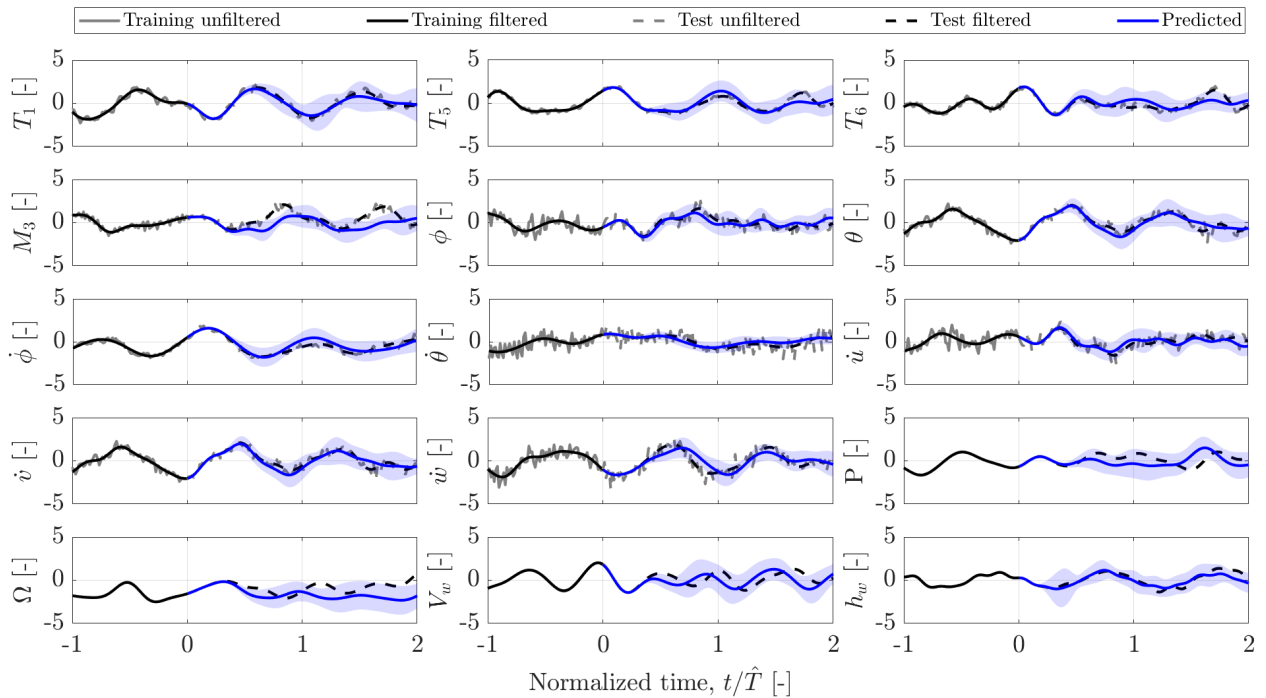


Figure 24: Filtered z-score data prediction, SHDMD approach, random predicted sequence n.211

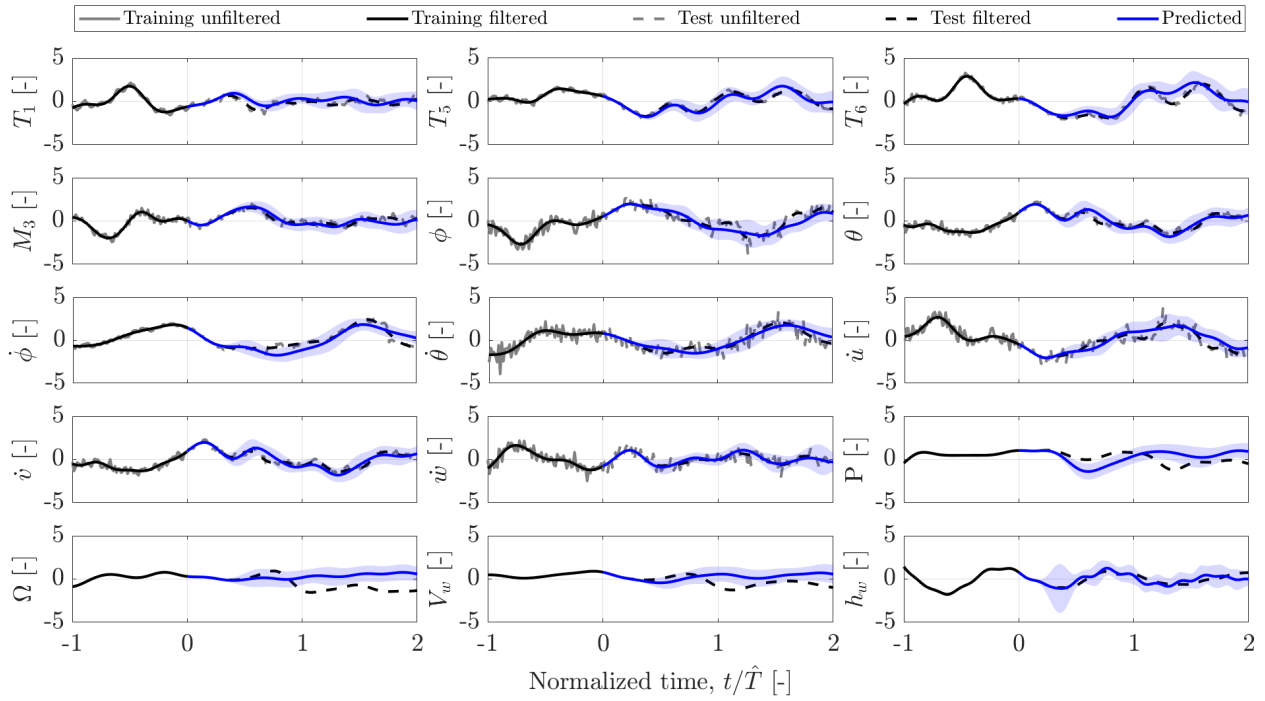


Figure 25: Filtered z-score data prediction, SHDMD approach, random predicted sequence n.223

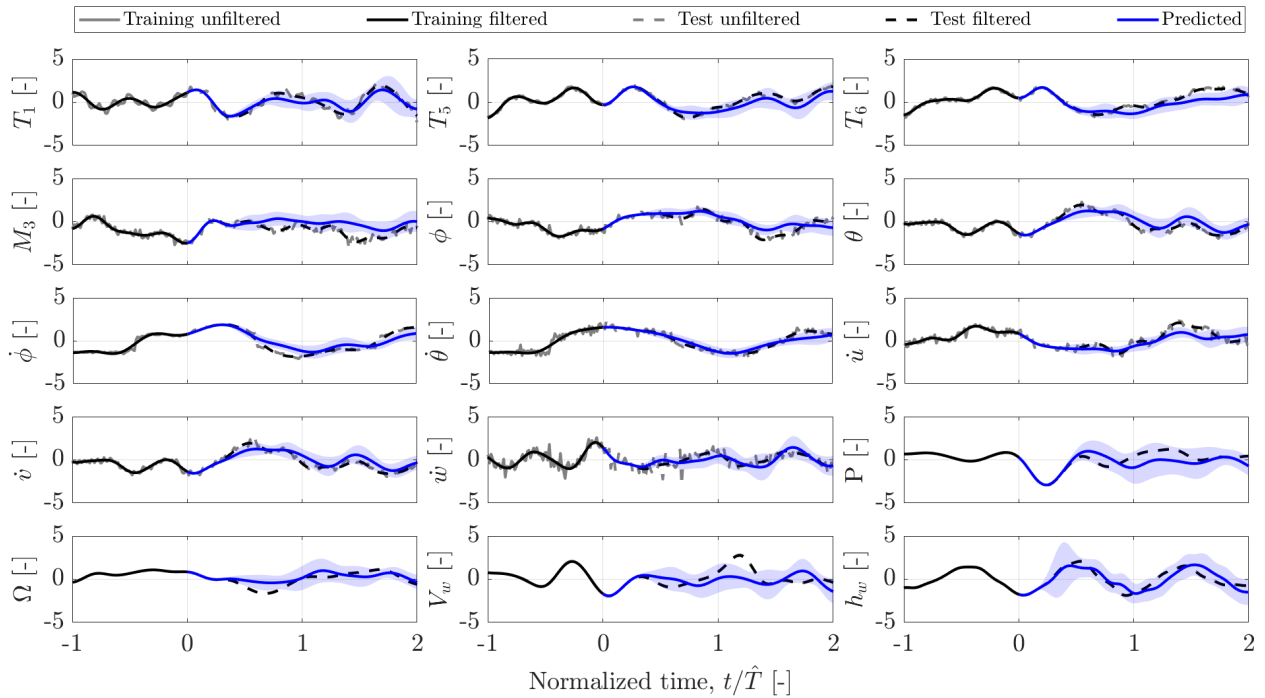


Figure 26: Filtered z-score data prediction, SHDMD approach, random predicted sequence n.240